AD-A170 782 LASER PRODUCED X-RAY FOR HIGH RESOLUTION LITHOGRAPHY AND A PHOTOIONIZATION LASER(U) BATTELLE COLUMBUS DIV OH H EPSTEIN ET AL. 14 FEB 86 AFOSR-TR-86-0553 1/1

UNCLASSIFIED AFOSR-82-0066 F/G 20/8 NL

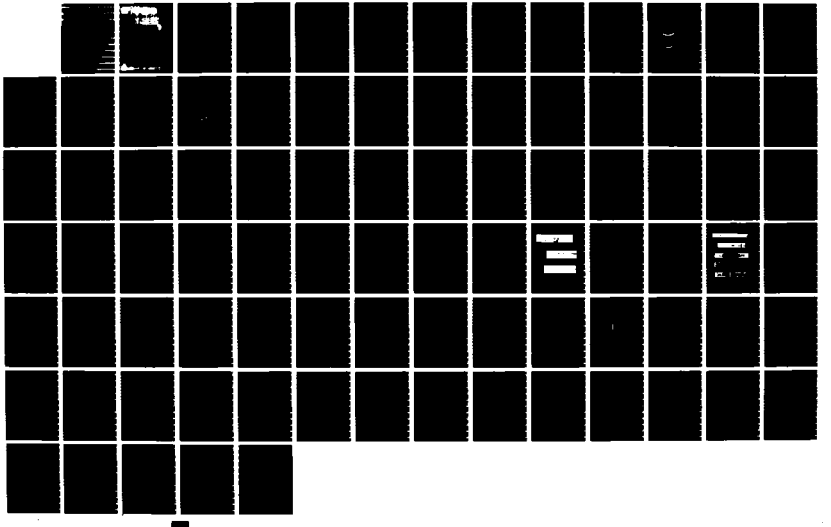

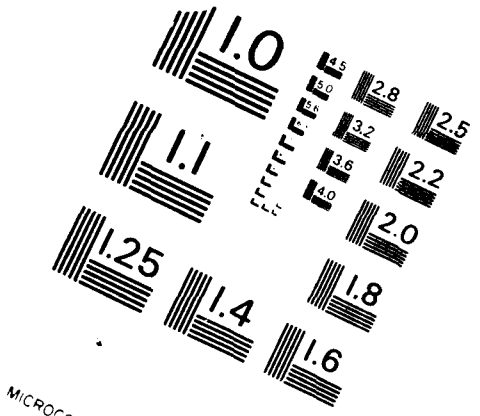

(2)

LASER PRODUCED X-RAY FOR HIGH RESOLUTION LITHOGRAPHY AND A PHOTOIONIZATION LASER

to

AFOSR
Bolling AFB
Washington D. C.

(2)

FINAL REPORT

on

Approved for public release,
distribution unlimited

LASER PRODUCED X-RAY FOR HIGH RESOLUTION LITHOGRAPHY AND A PHOTOIONIZATION LASER

to

AFOSR
Bolling AFB
Washington D. C.

February 14, 1986

from

Harold Epstein
Dave Applebaum
Bernerd Campbell

BATTELLE
Columbus Division
505 King Avenue
Columbus, Ohio 43201

UNCLASSIFIED
SECURITY CLASSIFICATION OF THIS PAGE

AD-A170782

REPORT DOCUMENTATION PAGE

1a. REPORT SECURITY CLASSIFICATION Unclassified	1b. RESTRICTIVE MARKINGS
2a. SECURITY CLASSIFICATION AUTHORITY	3 DISTRIBUTION / AVAILABILITY OF REPORT Approved for public release; Distribution unlimited
2b. DECLASSIFICATION / DOWNGRADING SCHEDULE	
4. PERFORMING ORGANIZATION REPORT NUMBER(S)	5. MONITORING ORGANIZATION REPORT NUMBER(S) AFOSR-TR- 86-0553
6a. NAME OF PERFORMING ORGANIZATION Battelle Columbus Division	6b OFFICE SYMBOL (If applicable)
6c. ADDRESS (City, State, and ZIP Code) 505 King Avenue Columbus, OH 43201	7a. NAME OF MONITORING ORGANIZATION AFOSR/NP
8a. NAME OF FUNDING / SPONSORING ORGANIZATION AFSOR	8b OFFICE SYMBOL (If applicable) NP
8c. ADDRESS (City, State, and ZIP Code) Building 410 Bolling AFB DC 20332-6448	7b ADDRESS (City, State, and ZIP Code) Building 410 Bolling AFB DC 20332-6448
	9. PROCUREMENT INSTRUMENT IDENTIFICATION NUMBER AFOSR 82-0066
	10 SOURCE OF FUNDING NUMBERS

PROGRAM ELEMENT NO	PROJECT NO	TASK NO	WORK UNIT ACCESSION NO
61102F	2301	A8	

11. TITLE (Include Security Classification)
"LASER PRODUCED X-RAY FOR HIGH RESOLUTION LITHOGRAPHY & PHOTOIONIZATION LASER"

12. PERSONAL AUTHOR(S)
Drs Harold Epstein, Dave Applebaum, & Bernerd Campbell

13a. TYPE OF REPORT	13b. TIME COVERED	14. DATE OF REPORT (Year, Month, Day)	15. PAGE COUNT
FINAL	FROM 15 Dec 81 TO 14 Dec 85	Feb 14, 1986	67

16. SUPPLEMENTARY NOTATION

17. COSATI CODES			18. SUBJECT TERMS (Continue on reverse if necessary and identify by block number)
FIELD	GROUP	SUB-GROUP	

19 ABSTRACT (Continue on reverse if necessary and identify by block number) The majority of the project was spent investigating laser-produced x-rays for high resolution lithography. This work involved measurements over an extensive parameter matrix. Specifically, efficiency of conversions to x-rays was qualified as a function of (1) laser pulse energy, (2) laser pulse width, (3) plasma profile, (4) laser wavelength, (5) target atomic number, (6) initial focal area, and (7) focal ratio of the lens. During the last eighteen months of the program, experimental research was performed on a photionization x-ray laser concept. Specifically, a thin polyethylene, oxidicarbonate film was vaporized. Fifteen nanoseconds into its expansion, the vapor was illuminated by a 200 psec Fe spectrum x-ray pulse. Photoionization of the inner K-shell of oxygen was then observed. The potential efficiency of this type of laser was found to be comparitively low.

20 DISTRIBUTION / AVAILABILITY OF ABSTRACT	21 ABSTRACT SECURITY CLASSIFICATION
☒ UNCLASSIFIED/UNLIMITED ☐ SAME AS RPT ☐ DTIC USERS	Unclassified

22a NAME OF RESPONSIBLE INDIVIDUAL	22b TELEPHONE (Include Area Code)	22c OFFICE SYMBOL
Dr Robert J. Barker	202/767-4908	NP

DD FORM 1473, 84 MAR 83 APR edition may be used until exhausted
All other editions are obsolete

SECURITY CLASSIFICATION OF THIS PAGE
UNCLASSIFIED

TABLE OF CONTENTS

LIST OF FIGURES (Continued)

LIST OF TABLES

SECTION 1

A PHOTOIONIZATION X-RAY LASER

A PHOTOIONIZATION X-RAY LASER

INTRODUCTION

The ejection of electrons from inner shells of atoms through photoionization was first suggested by Duguay and Rentzepis[1] as a straightforward means of creating population inversions at vacuum UV and x-ray wavelengths. For example, when an electron has been ejected from the K-shell of an atom, the residual ion is left in an excited state which can decay by an L-shell electron dropping into the K-shell. Since there are no ions initially, the photoionization process has created a population inversion in a single step.

For x-rays with sufficient energy to remove an inner shell electron, the photoionization of the K-shell has a considerably higher probability than that of the L-shell, typically a factor of 10 for soft x-rays. Thus, the nature of the photoionization process gives a strong preference for the ejection of an inner shell electron. A relatively broadband x-ray source is clearly an effective pump for an x-ray laser. In contrast, impact ionization by electrons or ions does not appear to be well suited for selective removal of inner shell electrons[1-3] while photoexcitation requires a well matched x-ray line pump source.[3]

The most intense laboratory source of soft x-rays is the laser produced plasma. Battelle demonstrated the capability of converting giant Nd-glass laser pulses to x-rays in the 1 keV range with an approximately 20 percent efficiency in 1971.[4,5] At that time, Mallozzi suggested the laser plasma x-rays as a pumping source for an inner-shell photoionization laser.[4,6,7] The x-ray pump intensities available from laser plasma sources are of the order required for an x-ray laser of $\sim$1 keV based on photoionization of K- or L-shells.

The 100 picosec to 1 nanosec pulse widths characteristic of most of the giant pulsed lasers are essentially C-W compared to the femtosecond lifetimes of the excited states. A criterion which is obeyed in almost all C-W lasers is that $\tau_u/\tau_1 > g_u/g_1$, where $\tau_{u,1}$ are the lifetimes of the upper and lower laser states of statistical weights g. This condition is not satisfied

for the Kα lines in most low atomic number materials,[8] which would indicate that population inversions would terminate in a time of the order of the lifetime of the vacancies and that pumping pulse widths of 10^{-14} to 10^{-15} seconds would be required. However, independent analyses by Mallozzi[9,10] and Stankevich[11] have shown that C-W laser action could be achieved by low atomic number elements. In the Auger decay of a K-shell vacancy, an L-shell electron is ejected from the atom. Since the final state has two L-shell vacancies, its energy level is displaced by tens of eV from the one vacancy state and is no longer resonant with the $K\alpha_1$ line. Since the total decay rate for K-shell photoionization in low Z elements is predominantly due to radiationless Auger processes that do not populate the lower laser levels, Mallozzi determined that a more applicable criterion is

$$\frac{\tau_{u\rightarrow l}}{\tau_l} > \frac{g_u}{g_l} \qquad (1)$$

where $\tau_{u\rightarrow l}$ is the radiation lifetime. This criteria is satisfied by many light elements.[6]

Since the ratio of statistical weight is 1/2 for the $K\alpha_1$ versus 1 for the $K\alpha_2$, the $K\alpha_1$ transitions offer a wider choice of elements capable of C-W lasing. This is particularly important when laser plasma x-rays are to be used as the pump source. It is relatively easy to produce an intense x-ray source with a plasma bremsstrahlung temperature of $\sim$ 1 keV, falling off exponentially with energy as $e^{-h\nu/kT}$. The decrease in the x-rays available for photoionization with increasing $h\nu$ combined with the increase in pumping power requirement make the choice of a very low atomic number element desirable. For example, almost an order of magnitude less laser power would be required to pump Na than Si. An 0.1 terrawatt laser system focused to 70 micrometers diameter should be adequate to test a Na photoionization laser concept. This power capability is available in a single beam of the Battelle 12-beam Nd-doped glass laser.

However, producing a medium with the states in the idealized condition assumed in the analyses may not be easy. A very high density of a specific ionic species, 10^{-3}-10^{-4}, must be achieved in the presence of Auger processes and possibly thermal ionization. There is little doubt that further research is required on the effects of Auger processes and time dependent thermal ionization on the distribution and energy levels of the ion species.[8]

BACKGROUND

Since the process of photoionization of an inner-shell electron creates an inversion in a single step, the feasibility of an x-ray laser depends primarily on whether or not the pumping can be sufficiently intense for the gain to exceed the absorption, and whether or not C-W laser action can be achieved. The cross section for stimulated emission, σ_s, is

$$\sigma_s = \frac{\lambda^2}{4\pi 2} \frac{\tau_{u\to l}^{-1}}{\Delta\nu} \tag{2}$$

where λ is the wavelength, $\Delta\nu$ is the linewidth, and $\tau_{u\to l}$ is the partial time constant for radiative decay from the upper to the lower state.

The line width is composed of the natural line width $\Delta\lambda_N$, the Doppler width $\Delta\lambda_D$, and the Stark width $\Delta\lambda_s$. The estimation of these three widths requires a knowledge of the plasma temperature and density. If one filters out the soft x-rays and allows a reasonable radiation geometry, the temperature will be low enough that the Doppler broadening $\Delta\lambda_D = \lambda\bar{v}/c$ is smaller than $\Delta\lambda_N$. The Stark broadening is very large at solid densities, but with the 15 nanosecond expansion planned for these experiments the plasma of interest can reach a density of $\sim 10^{20}$ or less. At this density, $\Delta\lambda_s$ is also smaller than $\Delta\lambda_N$ in the 10 Å wavelength regime.[10]

The gain G per centimeter is given by

$$G = \sigma_s(N_u - g_u/g_l\, N_l) \tag{3}$$

where N_u and N_l are the upper and lower state population densities, and g_u and g_l are the respective statistical weights.

The intended pump source is laser-plasma x-rays radiated from a plasma whose temperature is about 0.9 keV. If the laser is focused on a target with a multitude of L-lines just over 1 keV, the resulting x-rays will provide an effective pump source in the range from about 13keV to about 1.5 keV as shown in Figure 1-1. The elements for which photoionization of the K-shells appear most practical are O to Mg. Lower energy transitions to the K- or L-shells require less pumping power but thermal ionization becomes an increasingly severe problem.

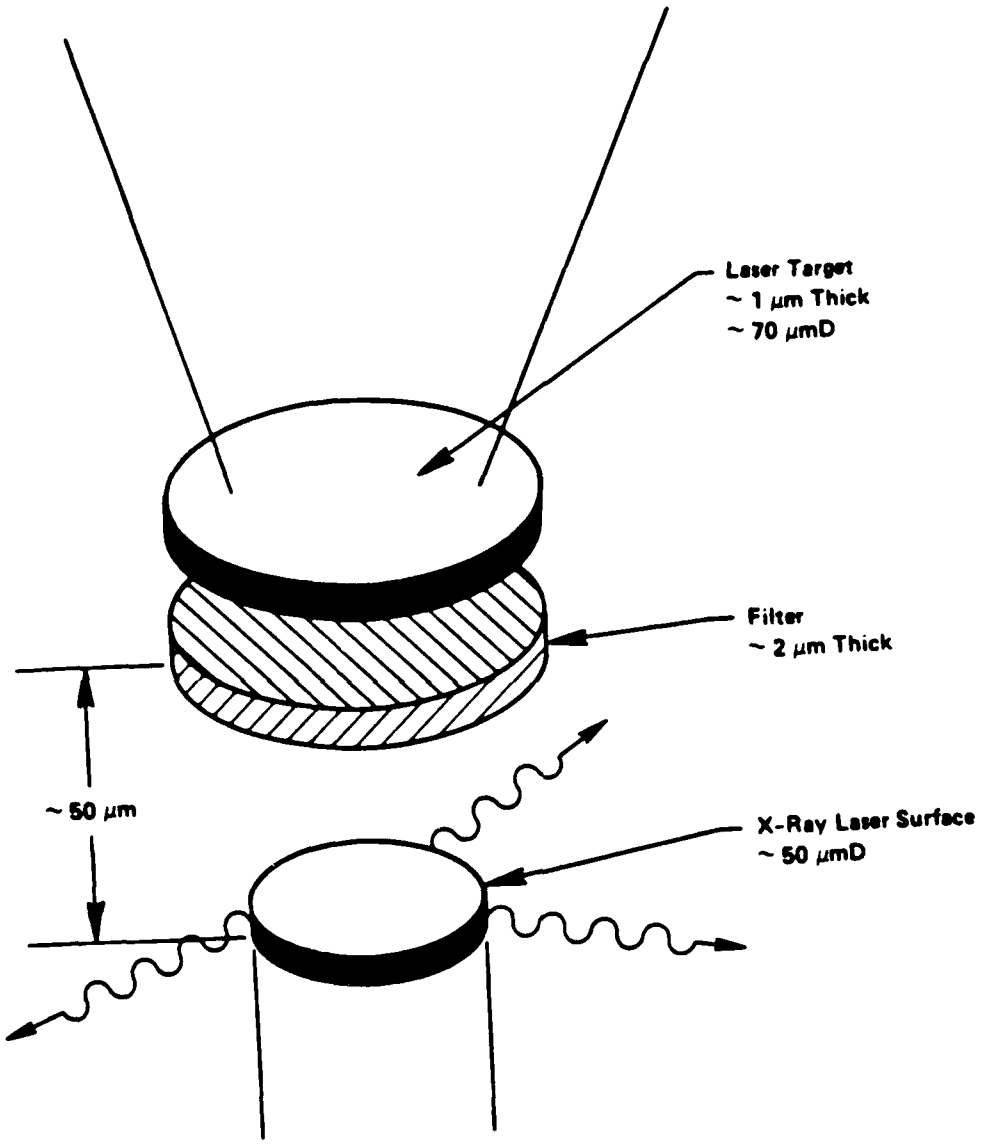

FIGURE 1-1. X-RAY LASER CONFIGURATION

Let us consider pumping a flat x-ray laser surface in the configuration of Figure 1-1. Assuming a cold Na target, the $K\alpha_1$ transition is at 1.04 keV. Substituting into Equation (1) we find

$$\sigma_s = \frac{(11.89\ \text{Å})^2}{4\pi^2} \frac{(8.3 \times 10^{-14}\text{s})^{-1}}{6.5 \times 10^{13}\ \text{Hz}} \tag{4}$$

$$= 6.6 \times 10^{-17}\ \text{cm}^2$$

In order to have a laser, the gain must exceed the absorption loss. For Na just below the K-edge, $\sigma_a = 2.2 \times 10^{-20}$. Thus, 3.3×10^{-4} of the Na atoms would have to be in the upper state. This estimate assumes cold, undisturbed Na. The actual situation is considerably more complicated.

Maintaining 3.3×10^{-4} of all the Na atoms in excited state (K-shell vacancies) requires enormous pumping power because of the short lifetimes associated with inner-shell vacancies. The ideal pump is to use x-rays of energy just above the K-edge of Na. Fortunately, it is possible to produce a source with very nearly this characteristic by filtering the laser-plasma x-rays with the right thickness of a low atomic number material such as carbon. The sharp decrease in x-ray transmission through the sample with decreasing energy provides a low energy "cutoff" while the x-ray source decreases exponentially with increasing energy. The result is a relatively narrow band of x-rays as shown in Figure 1-2, with the peak position determined by the thickness and composition of the filter. While the initial set of experiments utilize an 0 laser surface and no filter, a filter will be required at a later stage.

Let us calculate the x-ray energy transmittance of the filter assuming that x-rays emitted from the plasma follow the plasma bremsstrahlung envelope. This is a "worst case" assumption because any source tailoring will add x-rays in the effective pumping band. The energy density E_p through the filter is given by $E_p \simeq C_1 \int_0^\infty \exp[-\alpha\chi-(h\nu)/h\nu]dh\nu$ j/cm^2 where $\alpha(\text{cm}^{-1})$ and χ(cm) are the absorption coefficient and thickness of the filter, and C_1 is a constant depending on the laser pulse energy, pulse width, and target. For the 100 J, 1 nanosec pulse incident on a 100 micrometer disc used as a reference in this proposal, C_1 is approximately 2×10^5. For a water equivalent plastic filter, $\alpha \simeq 5000(h\nu)^{-3}$.

$$E_p \simeq 2 \times 10^5 \int_0^\infty \exp[-5000(h\nu)^{-3}\chi-(h\nu/kT]d(h\nu)\ \text{J/cm}^2 \tag{5}$$

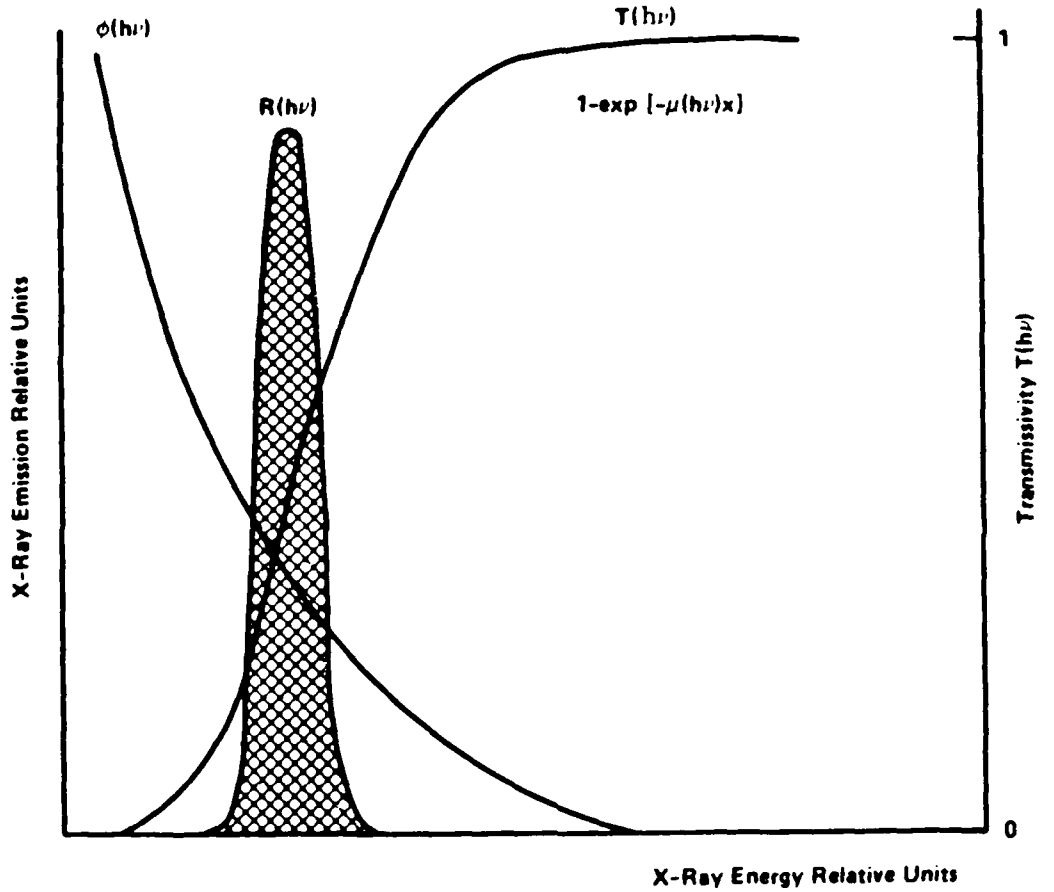

FIGURE 1-2. BAND PASS THROUGH X-RAY FILTER

The peak $(h\nu)_m$ of the x-ray transmission occurs at

$$(h\nu)_m \simeq 11\chi^{1/4}kT^{1/4} \tag{6}$$

Because of the sharply peaked integrand when kT is less than $(h\nu)_m$, the integral can be evaluated by expanding in a Taylor series about $(h\nu)_m$ (saddle-point method), giving

$$E_p \simeq 9 \times 10^5 (kT)^{5/8} \chi^{1/8} \exp[-14.7\chi^{1/4}/(kT)^{3/4}] \text{ j/cm}^2 \tag{7}$$

If we wish to have the peak occur at, say 1.2 keV, a filter thickness of 1.6×10^{-4} cm is required, yielding an E_p of 5×10^4 J/cm^2. With a 1 nanosec pulse, the x-ray pumping power is about 5×10^{13} w/cm^2. A gap between the filter and the x-ray laser surface is needed to avoid the interaction of photoelectrons.

The power flux P required to maintain a probability Ψ of finding a K-shell hole in a given atom is

$$P = \frac{\Psi\, h\nu\, \tau_u^{-1}}{\sigma_p} \tag{8}$$

where σ_p is the K-shell photoionization cross section and τ_u^{-1} is the total decay rate of the upper level. We can now estimate the x-ray flux required to pump a cold Na K-shell photoionization laser.

$$P = \frac{3.3 \times 10^{-4} \times 1.1 \text{ keV}}{2.2 \times 10^{-19} \text{ cm}^2 \times 2.8 \times 10^{-15} \text{ sec} \times 6 \times 10^{15} \text{ keV/J}}$$
$$= 1.1 \times 10^{14} \text{ w/cm}^2 \tag{9}$$

The required pumping power is somewhat higher than is currently available with laser plasma x-rays. However, the threshold pumping power scales inversely as the cube of wavelength for a cold medium. Substituting a dominantly oxygen lasant for the sodium would provide about a factor of seven improvement. With a lower atomic number lasant, it may be possible to omit the filter and use a laser-plasma K-line emitter, such as Mg, for the pump source. With frequency tripled or quadrupled Nd laser light, the efficiency for producing these x-rays is in the range of 2 or 3 percent, making pumping powers of over 10^{13} w/cm^2 likely and simplifying the experimental configuration.

Furthermore, the cold lasant assumption is, in many ways, a worst case. The principal contributions to the line width are the Auger transition. Removing L-shell electrons by ionization can narrow the line width considerably.[12] Of course, it is necessary to have at least one L-shell electron for the inner-shell photoionization inversion to apply. If Auger transitions were eliminated, $\tau\Delta(h\nu)$ could approach the Heisenberg limit of τ and Equation (2) would become

$$\sigma \approx \lambda^2 \quad .$$

This would be more than a 2 order of magnitude improvement. (This ideal case is, of course, not really attainable.) In addition, the removal of outer shell electrons substantially lowers the absorption cross section below the K-edge of sodium, providing almost another order of magnitude improvement in threshold pumping power.

On the other hand, several disadvantages must be considered when a hot plasma is created. First, Doppler broadening, $\Delta\lambda_D$, may dominate the line width

$$\Delta\lambda_D = \frac{\lambda\bar{v}}{C}$$

where $\bar{v}$ is the average thermal velocity of the ion. The optimum temperature to form the Li-like state of Na in a Coronal plasma is approximately 40 eV.[13] At this temperature, the Doppler line width dominates the reduced natural line width, but the cross section σ_s is a factor of 6 higher than that given by Equation (4). It is also possible to heat and ionize the plasma with a prepulse a few nanoseconds before the x-rays. The expansion cooled plasma would "freeze" in a nonequilibrium ionization with a lower Doppler broadening.

The second disadvantage of the hot plasma is that it is also necessary to consider Stark broadening in the highly ionized plasma. The electron density would have to be reduced below $\sim 10^{20}$ electrons/cm^2 before pumping with x-rays. With the lower density, a greater active length is required to give adequate gain.

The third disadvantage of a deeply ionized plasma is that more than one ionization state is present in the plasma. Only the predominant state contributes to the threshold. Furthermore, for the more highly ionized states, thermal population of the lower level decreases the inversion density.

EXPERIMENTAL PROGRAM

Photoionization pumping of an x-ray laser based on a lasant in the plasma state differs substantially from photoionization pumping of a cold lasant suggested by Duguay, et al. With a cold material, a single photoionization event creates an inversion because there is no steady state population in the lower laser level. This can be seen from Figure 1-3.

To a first approximation, Auger decays of the K-shell vacancy do not populate the lower laser level. The first step in an Auger cascade leaves the atoms with two vacancies. The ion is not a resonant absorber at the $K\alpha$, wavelength because the additional vacancy shifts the absorption line up in energy by about 20 eV.

The problem with the cold lasant concepts is that 10^{-2} to 10^{-3} of the atoms must be in the upper laser level to achieve gain. Because of the competing Auger process, the power required to achieve this level of inversion is much higher than for the partially ionized atoms. It is almost impossible to maintain an unionized lasant with the required pumping power.

In the case of a hot plasma, the lower laser level can be populated by thermal ionization, reducing the potential inversion level. Since the fraction of oxygen ions expected to be pumped into the upper level is about 2×10^{-3}, the ratio n_{i+1}/n_i must be less than 10^{-3}, if lasing on the Li-like species is sought. A temperature below 11 eV is needed (Figure 1-4). At 11 eV only 2% of the ions are Li-like. The Be-like ions are more promising. While the temperature must be below 8.4 eV, about 25% of the ions are Be-like at this temperature.

Figure 1-5 shows the length of time that each ion species is dominant and the maximum flux during this time. From this figure, the He-like lines should be almost an order of magnitude stronger than the Li-like, while the Be-like should be about 30% weaker than the Li-like.

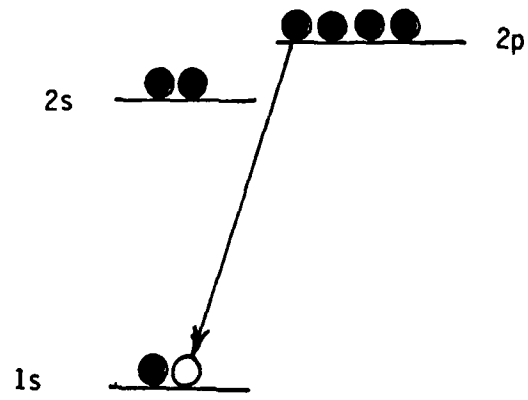

FIGURE 1-3. ELECTRONIC STRUCTURE OF O WITH ONE K-SHELL VACANCY

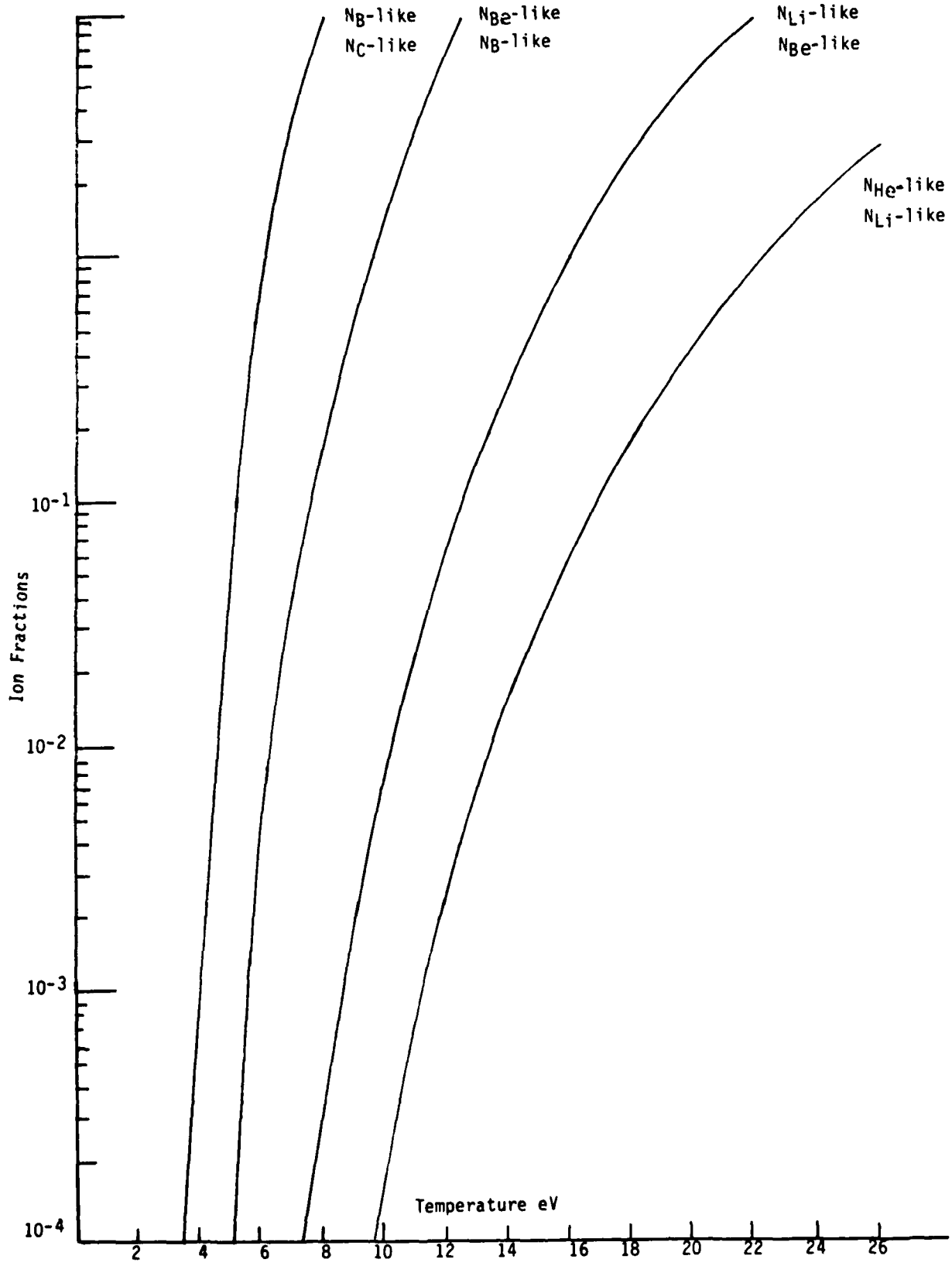

FIGURE 1-4. ION SPECIES RATIOS OF OXYGEN

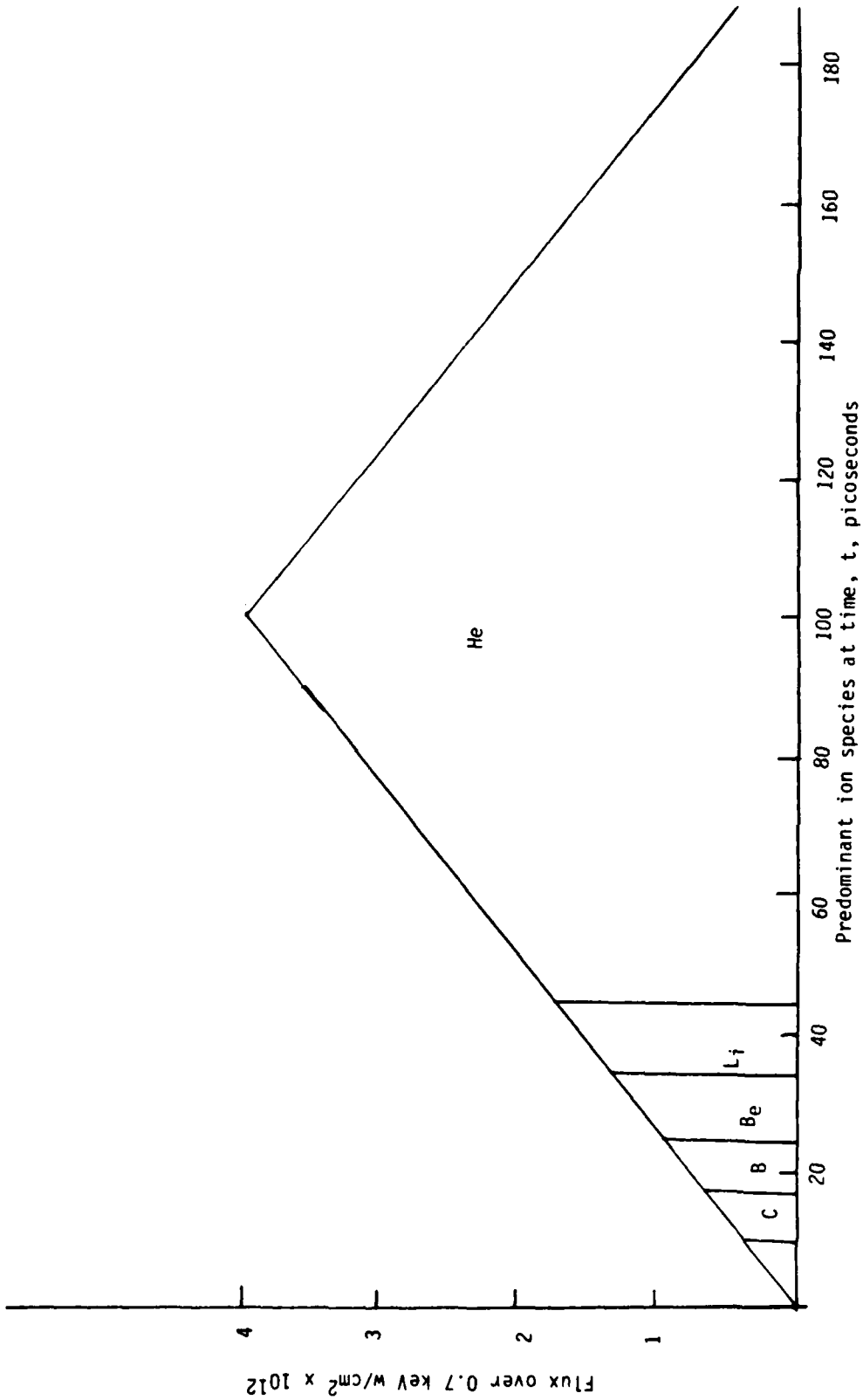

FIGURE 1-5. PUMPING FLUX AND TIME FOR PREDOMINANT ION SPECIES, TRIANGULAR APPROXIMATION OF PULSE

The main problem is designing a target that will have the proper temperature and density when the pumping pulse is initiated. The target starts out with a solid density of $\sim 10^{23}$, so an expansion of about 3 orders of magnitude is needed before the x-ray pumping pulse is initiated. At a typical initial vapor temperature, the velocity will be $\sim 2 \times 10^5$ cm/sec. If a target is 1 μm thick and a line focus is used to create the oxygen, the vapor will expand to the correct density in about 15 nsec.

The experimental geometry is shown in Figure 1-6. The oxygen vapor is created by a beam split off after the second YAG amplifier. The energy in this beam is ~10 mJ. The remainder of the laser beam goes through 4 Nd doped glass amplifiers to produce a pulse of ~25 J with a pulse width of 200 psec. The time delay is approximately 15 nsec.

The x-ray laser materials would ideally be pure oxygen, although heat capacity considerations make the addition of lower Z atoms advantageous. Building and working with a thin cryogenically cooled target presents problems beyond the resources of this program. The best alternative appears to be a carbonate target. In particular, polyethylene oxidecarbonate of the form

$$(- \underset{\underset{O}{|}}{C}H_2 - CH_2 - O - \overset{\overset{O}{\|}}{C} - O -)$$

is 61.5 percent oxygen by weight. This compound can be dissolved in chloroform and cast in the form of a thin film on water.

The geometry chosen for the target is shown in Figure 1-7. The thin polyethylene oxidicarbonate film is vaporized approximately 15 ns before the x-ray pulse. This allows the vapor to expand to a density corresponding to $\sim 10^{20}$ oxygen atom per cm^3 to limit the Stark broadening of the x-ray lines. The initial vapor is formed as a line 1.5 mm long by 0.15 mm in diameter. In 10 ns this expands into a cylindrical plasma ~1.5 mm long with a flat elliptical cross section 15 mm in major axis by ~.01 mm in minor axis. The x-ray source is an ~200 psec pulse

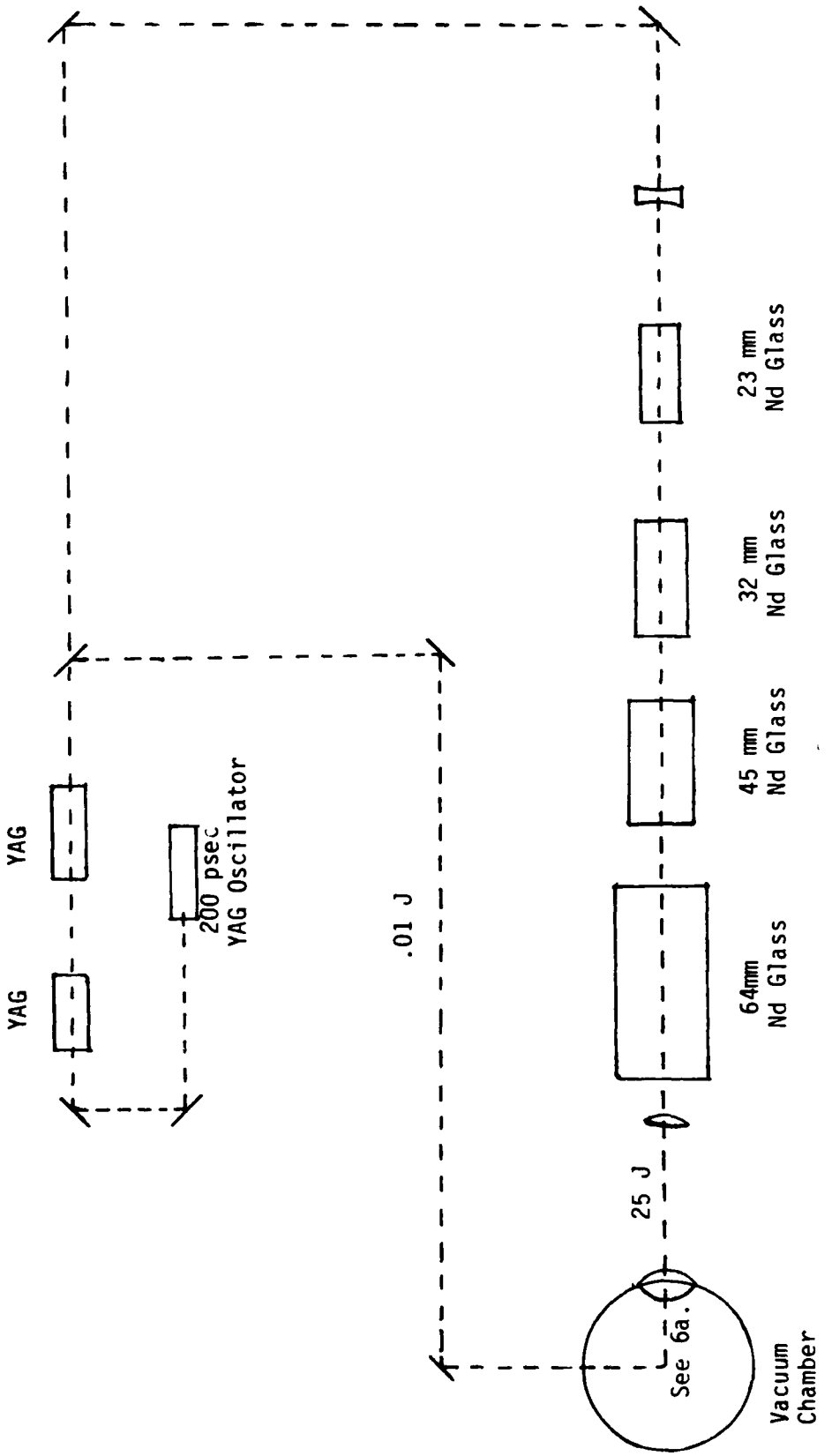

FIGURE 1-6. BEAM SCHEMATIC

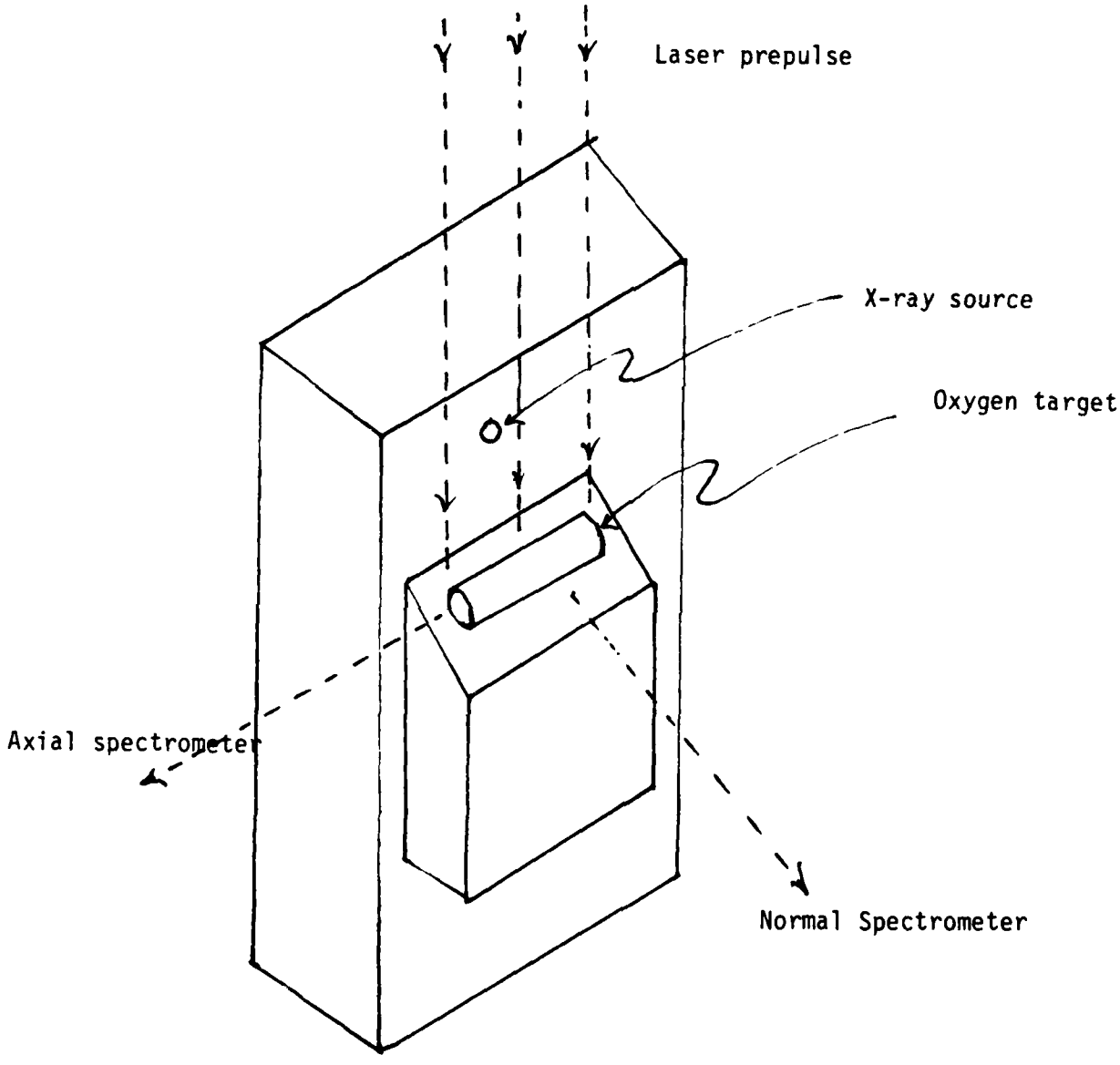

FIGURE 1-7. TARGET CONFIGURATION

with the Fe spectrum shown in Figure 2-8. The L-resonance lines at 725 and 737 L-eV are very well matched for efficiently photoionizing the K-shell of oxygen.

The x-ray source has a diameter of ∿.15 mm and is produced at a sufficient distance to prevent the high-energy laser-plasma from interacting with the O before the x-ray pulse is over. Since the plasma moves at a speed of $\sim 2 \times 10^7$ cm/sec the x-ray source must be at least 4×10^{-2} cm from the O vapor. This distance was chosen to be 0.4 cm. With a 20 J laser pulse and a 10% conversion efficiency, that produces an x-ray flux of $\sim 2 \times 10^{12}$ W/cm^2 to pump the O plasma. While the efficiency for the production of x-rays with sufficient energy to pump the photoionization level of O is ∿10%, the overall efficiency of x-ray and X-UV radiation is ∿50% or 10^{13} W/cm^2.

The cylindrical target geometry was chosen instead of the disc geometry discussed in the background because in the absence of the filter it is preferable for diagnostics.

The following is further evaluation of the necessary conditions for measurable gain in a photoionization pumped x-ray laser. Such effects on the line width as ionization of the outer electrons, Doppler broadening, and Stark Broadening will be considered in this section. With this information an optimum temperature and particle density range can be selected. The gain coefficient corresponding to this optimum will then be calculated. As duscussed previously, fraction of the atoms in the desired Li-like species decreases exponentially with increasing temperature[13], and it is important that the temperature be kept below 25 eV for oxygen.

It is relatively easy to heat the plasma to this temperature; the problem is to remove enough of the excess energy supplied by the x-ray pump source to prevent the x-ray laser from overheating. There are three mechanisms to limit the temperature rise of the oxygen plasma: thermal conductivity, thermal radiation, and heat capacity.

The thermal conductivity K is given by

$$K = (2/\pi)^{3/2} \frac{20}{\ell n \Lambda} \frac{k(kT)^{5/2}}{m_e^{1/2} e^4} \times 10^{-7} \text{ Watt/cm}^2 \text{ °K/cm}$$

where Λ is

$$\frac{3}{2e^3} \left(\frac{k^3 T^3}{\pi n_e}\right)^{1/2}$$

At a temperature of 25 eV or 2.9×10^5°K, the heat loss due to thermal conductivity is negligible compared to the input power from the pump source.

The radiant heat transfer, P_R is given by

$$P_R = 6.7 \times 10^{-12} T^4 \text{ W/cm}^2 \text{ °K}$$

if the plasma is a black body radiator. At a temperature of 25 eV, there is good reason to believe that the plasma will be almost a black body radiator. At any rate, this will give an upper limit to the heat removal which can be expected from radiation. Assuming one sided radiation, because the x-ray source will probably block radiation from the other side, the allowable pumping power input, P_i, is 5×10^{10} W/cm^2. If 2/3 of the absorbed x-ray energy is emitted as Kα radiation, then P_i can be increased to 6×10^{10} W/cm^2. If the x-ray laser is initially 1 μm thick and has an initial density of 1 gm/cm^3 and 50 weight percent oxygen (the remainder is H and C), then P_i becomes $\sim 7 \times 10^{10}$ when transmitted energy is subtracted off. This is still not enough pumping power to give a reasonable gain.

The alternative is to use a mode-locked laser pulse and depend on the effective heat capacity to prevent an excessive temperature rise.

For Li-like ions at 22 eV, the energy per atom in a pure O target without a filter is given by:

$$E_{ox} = \bar{\sigma}_{ox} \times \bar{\phi}\, t = F_{therm} + E_i = 426\text{eV}$$

where

$$\bar{\sigma}_{ox} = \int_0^\infty \sigma_{ox}(E)\, \phi(E)\, dE \quad .$$

This assumes a square pulse. With a triangular pulse, about twice the average power is desirable so the Li-like plasma occurs at the peak flux. This allows an average flux of $\sim 2 \times 10^{12}$ W/cm^2. The actual average flux of $\sim 10^{13}$ W/cm^2 creates a H-like and He-like plasma. With the cooling effect of the additional element included the plasma becomes more He-like at $\sim$125 eV.

As discussed in the section on inversion conditions, this temperature is far higher than optimum. The temperature can be reduced considerably by adding a low atomic number filter to absorb the $\sim$80% of the soft x-rays whose energies are too low to pump the K-shell photoionization in oxygen. However, the filter must be far enough away from the O layer to prevent the photoelectrons produced in the filter from interacting with the O target and destroying the inversion. The absorption characteristics of the filter are discussed in the section on filters. The decrease in the effectiveness of the filter as the filter becomes an increasingly ionized plasma is not considered.

A second method of maintaining the O plasma at a reduced temeprature is to add low atomic number elements such as hydrogen with the O. Duguay[14] suggested adding solid hydrogen in crystals. The buffer atoms would not absorb an appreciable amount of the x-ray energy capable of photoionizing O, but would increase the effective heat capacity of the target. Actually, increasing the hydrogen content in the chemical compound comprising the O film has about the same effect.

The third method is to utilize a shorter laser pulse to produce the same flux. The disadvantage of this alternative is that the energy on the spectrometer would be relatively low, making the diagnostics difficult.

It is suggested that in future experiments one or a combination of the three above modifications be made to increase the inversion density in the lower temperature ion states of interest.

Since the outer electrons are stripped to Li-like and He-like states, absorption of the Kα line should be very low. The gain coefficient is, therefore, given by

$$\alpha \approx \sigma_s N_u$$

where

$$\sigma_s = \frac{\lambda^4}{4\pi^2} \frac{\tau_{u=\ell}^{-1}}{3 \times 10^{10} \Delta\lambda} = 8.2 \times 10^{-16} \text{ cm}^2$$

At 25 eV, the Doppler broadening is 1.25×10^{-3} Å ($\Delta\lambda_D = \frac{\lambda \bar{v}}{c}$) for oxygen with $\lambda_0 = 21.55$ Å. The natural line width for the Li-like species is a few times 10^{-4} as seen in Figure 1-8,[8] and the Stark broadening can be neglected below $(n_e n_i)^{1/2} \approx 10^{20}$ as shown in Figure 1-9.[8] The number density of ions in the upper level, N_u, is given by

$$N_u = \frac{P_i \sigma_p \tau_u N \times 6 \times 10^{18}}{h\nu}$$

where τ_u is the total life time of the upper lever. Since we have eliminated most of the Auger transitions, we can estimate that $\tau_u \approx \tau_{u-\ell}$ which we have taken to be 1.4×10^{-13} sec. The maximum value of N is limited by Stark broadening to $\sim 10^{20}/\text{cm}^3$. In order to produce a Li-like inversion $N_{He}/N_L < 10^{-3}$ or a temperature below 11.6 eV is required. At this temperature $N_{Li} \approx 5 \times 10^{18}$, and $Pi \approx 1.4 \times 10^{12}$

$$N_u \approx \frac{1.4 \times 10^{12} \times 3 \times 10^{-19} \times 1.4 \times 10^{-13} \times 5 \times 10^{18} \times 6 \times 10^{18}}{6 \times 10^{2}}$$

$$\approx 2.9 \times 10^{15}$$

and

$$\alpha \approx 8 \times 10^{-16} \times 2.9 \times 10^{15} \approx 2.4 \quad .$$

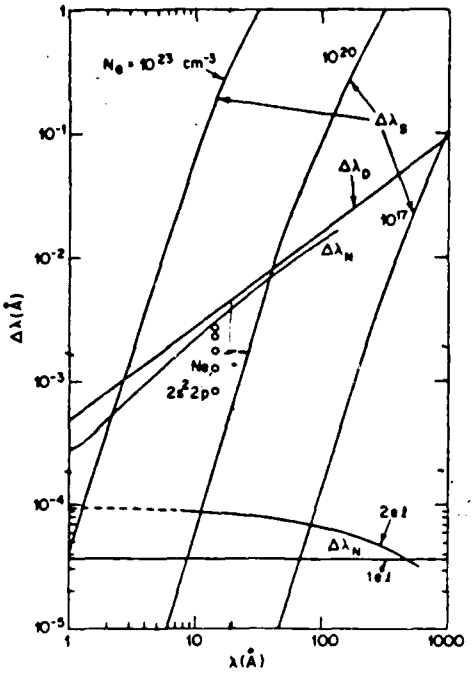

FIGURE 1-8.

Estimates of line widths for $K\alpha$ type transitions versus wavelength λ, with natural ($\Delta\lambda_N$), Doppler ($\Delta\lambda_D$), and Stark ($\Delta\lambda_S$) effects included. The decrease in natural broadening with ionization is indicated by circles for neon; and hydrogenic and helium-like ionic species are included (12)

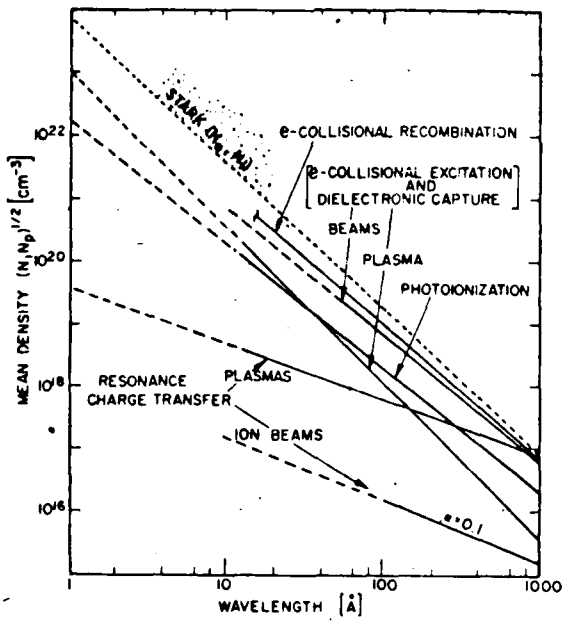

FIGURE 1-9.

Mean particle densities (solid and dashed lines) versus wavelength for selected pumping mechanisms and for a gain factor of $\alpha = 5$ ($\alpha = 0.1$ for ion beams). Stark broadening becomes important for large charged particle densities (same scale) in the region above the dotted line, also a region of approaching collisional equilibrium. Collisional recombination is plotted for fixed $N_e = 10^{21}$ cm^{-3} and terminates at ~15 Å due to dominance of radiative recombination to lower levels (12)

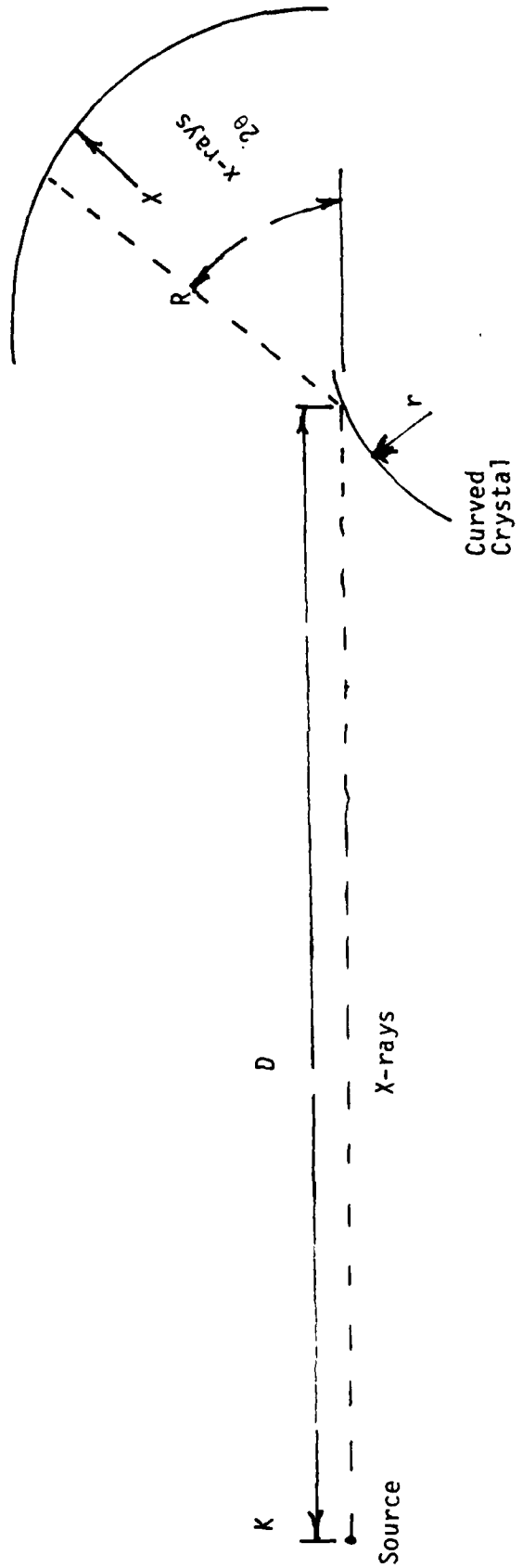

FIGURE 1-10. CURVED CRYSTAL SPECTROMETER

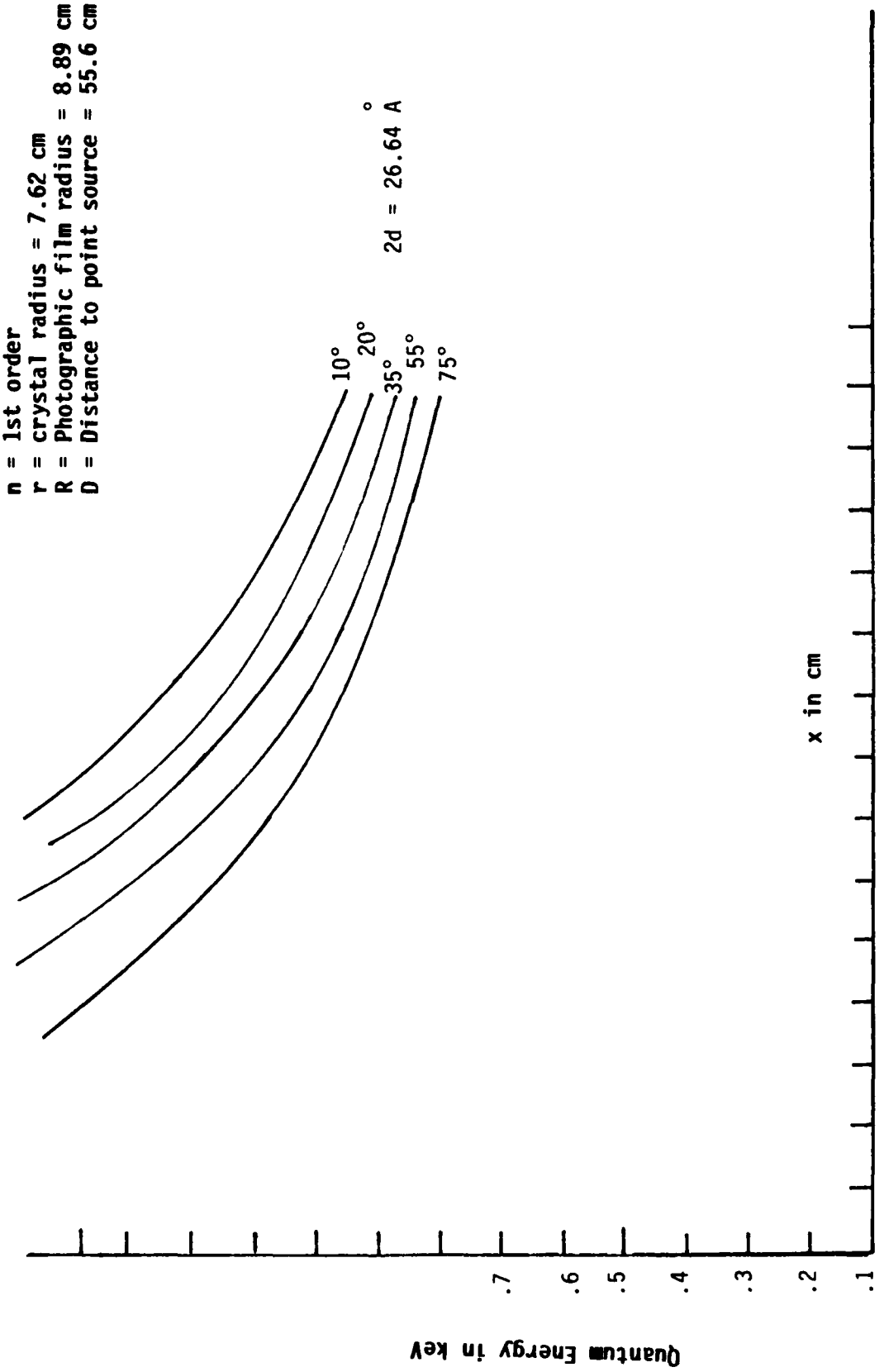

FIGURE 1-11. CALIBRATION CURVES FOR CONVEX BENT CRYSTAL SPECTROMETERS

RESULTS

The resonance lines of O VIII and O VII given in Table 1-1[11] have been observed along with several emission and absorption satellites. However, no lines from the lower ionization states of O have been identified. The recording film is the most sensitive available, so the primary options for improved sensitivity require a decrease in the effective resolution of the spectrometers. The pumping levels during the times that the plasma is in the ionization states of greatest interest are not high enough for measurable gain to be expected.

Exploritory experiments were carried out to examine optical depth effects and experiment geometry in oxygen laser produced plasma. Preliminary results indicate that both photo pumping and emission has been observed in Li-like species. Although specific line identifications require confirmation, these results are encouraging since they indicate the attainment of plasma conditions producing sufficient optical depth for absorption of pumping photons.

The tenative identification for these lines involve Li-like satellites to the He-like resonance:

$1s^2 - 1s2p$	He-like
$1s^22p - 1s\ 2p^2$	Li-like
$1s^22s - 1s^2s^2p$	Li-like .

These satellites represent doubly excited states which can be obtained through dielectronic recombination and autoionization processes. The observation of absorption lines in our experiments with the classic profile of Figure 1-12 is indicative of photoabsorption via the latter process.

Clearly the experiment in geometry is complex involving steep gradients in at least one dimension for electron density and temperature. Adjustment of the geometry for optimized optical path and state variables remains to be accomplished before observation of gain can be expected.

TABLE 1-1. OXYGEN LINES

Wavelength Å	Species	Transition
16.0	O VIII	$1s^2S_{1/2} - 3p^2P_{3/2,1/2}$
17.7	O VII	$1s^2\ ^1S_o - 1s4p\ ^1P_1$
18.6	O VII	$1s^2\ ^1S_o - 1s3p^1P_1$
18.9	OVIII	$1s^2S_{1/2} - 2p^2P_{3/2,1/2}$
21.55	O VII	$1s^2\ ^1S_o - 1s2p^1P_1$

A puzzling experimental result is that the $1S^2\ {}^1S_0$ - 1S 2p $^1P_1$ resonance line as seen by the axial spectrometer decreases as the laser energy increases above 20 J and disappears for laser energies above ∿30 J. This effect is not seen in the perpendicular spectrometer. It is speculated that the region of the plasma observed by the axial spectrometer ionizes beyond the O VII level. However, another explanation may be that the increase in recombination background radiation may make the opacity broadened line in the axial direction submerge in the noise.

The experimental configuration should produce a geometrical efficiency of .03 for the Fe x-rays to intercept the O vapor, and an 0.1 absorption efficiency for the x-ray above 0.7 keV. If 1/2 of the absorbed energy comes out as the O VII resonance line, this would mean that .0013 J is radiated in this line. This line was measured with a flat crystal spectrometer whose film plane was a distance of 45 cm from the source. The efficiency of a typical KAP crystal at the peak of its rocking curve at this energy is 5 percent. Therefore, the energy fluence reaching the film might optimistically be expected to be 0.06 erg/cm^2. The measured fluence at the film plane was .04 erg/cm^2, which shows that the plasma is indeed being pumped at the level needed to produce significant gain, if the plasma temperature can be lowered.

Plasma Temperature

The evaluation of the average temperature of the plasma emitting the visible lines is essential to characterize the region of x-ray emission. Because of the question of whether coronal steady state has been reached in the plasma, comparison of the resonance lines of the He and H-like species may err in the direction of under estimating the temperature. However, the comparison of different transitions within the same species can be strongly influenced by resonant photoexcitations. Since non steady state effects tend to cause relatively small errors the temperature is estimated by comparing the ratios of the He and H-like resonances. This temperature of 125 eV compares reasonably with the temperature determined from the width of the He-like resonance line assuming Doppler broadening dominates.

This temperature is, unfortunately, an order of magnitude higher than was desired. Effectively, the plasma passed through the temperature regimes of interest with maximum flux levels too low to be observed on the recording film of the spectrometers. Since the principal temperature control is the effective heat capacity of the plasma, the experiments requires a shorter pulse width to achieve a condition where the maximum flux occurs while the plasma is in the Li-like or Be-like state. Filtering out those x-rays which do not contribute to the photo-ionization would help, but a filter alone would not be sufficient.

In our experiment, the potential gain length is 0.4 cm giving us a potential gain coefficient of .96 or a gain of 2.6. This is marginal for experimental observation.

Instrumentation

The primary instruments for these experiments are two KAP crystal x-ray spectrometers, with convex curved or flat crystals. One of these spectrometers is looking along the axis of the cylinder and the other is normal to the axis. If there is gain in the oxygen plasma laser medium, the axial spectrometer will show an enhanced K line. This effect can be further verified by changing the length of the active medium.

The basic experiments utilize flat KAP crystals with a 2d spacing of 26.64 Å. However, some ranging experiments substituted curved crystals which provide a broad spectral record. The curved crystal geometry is shown in Figure 1-10, and wavelength calibration curves for KAP are shown in Figure 1-11.

Spectroscopy

The resolution of the flat crystal was adequate to show the Fano distribution (Figure 1-12),[15] of the first short wavelength absorption satellite of the $1s^2\ {}^1S_0$ - 1s 2p ${}^1P_1$ O VII transition or about 10^{-3} Å. The resonance line as seen in the spectrometer looking axially along the trial x-ray laser is considerably broader ($\sim 10^{-2}$ Å) than the same line in the spectrometer with a perpendicular view ($\sim 3 \times 10^{-3}$ Å). This has tentatively been attributed to opacity broadening, although instrumental explanations have not been ruled out.

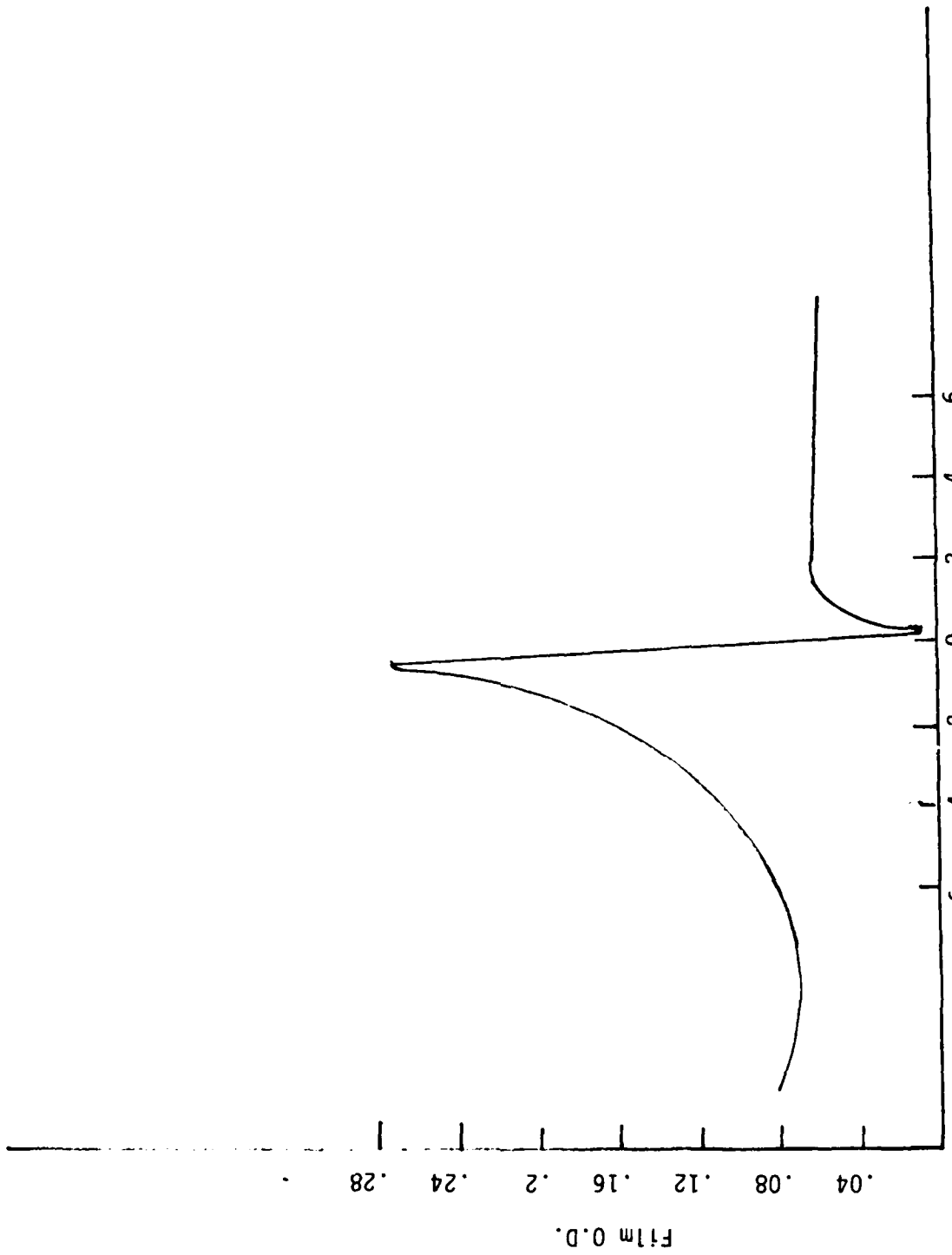

FIGURE 1-12. DISPLACEMENT FROM PEAK Å x 10^3

CONCLUSIONS

The pumping levels required for measured gain are achievable with a laser plasma x-ray source. However, the plasma heating is too great to allow the confirmation of gain on the present experiments. Four modifications can be considered to control the plasma temperature.

(1) Use a shorter laser pulse to permit the peak flux to occur at the desired temperature. Little pulse width flexibility is available in the present experiments.

(2) Insert a low-atomic number filter between the laser-plasma x-ray source and the oxygen target. This considerably complicates the target fabrication and requires the prepulse to come in from the side opposite the x-rays.

(3) Include a much larger low-heat sink in the oxygen target.

(4) The laser-plasma x-ray target can be a low-atomic number K-line emitter. A frequency doubled or tripled laser beam would probably be required to achieve the required x-ray conversion efficiency. A higher brightness laser would be advantageous for this alternative.

The potential efficiency of this type of x-ray laser is comparatively low. About 10 percent of the incident laser energy is converted to x-rays of energy sufficient to pump the levels of interest. About 3 percent of the O ions are in the Li-like state of a temperature where an inversion is possible. Finally, only about 4 percent of the pumping photons occur during the time interval while the plasma is in the correct ionization state. This efficiency can be improved considerably if the plasma temperature is controlled so that a much larger fraction of the photon pumping is done while the ionization states can lead to inversions.

REFERENCES

(1) Duguay, M. A., and Rentzepis, P. M., Appl. Phys. Lett., 10, 350 (1967).

(2) McCorkle, R. A., and Joyce, J. M., Phys. Rev. A., 10, 903-912 (1974).

(3) Hagelstein, Y. L., "Review of Radiation Pumped Soft X-Ray Lasers" Plasma Phys., Vol. 25, No. 12, pp. 1345-67, 1983.

(4) Mallozzi, P. J., Epstein, H. M., June, R. C., Applebaum, D. C., Fairand, B. P., and Gallagher, W. J., "X-Ray Emission from Laser Generated Plasmas", in Fundamental and Applied Laser Physics: Proceedings of the Esfahan Symposium (edit. by M. S. Feld, A. Javan, and N. A. Kurnit), John Wiley & Sons, Inc. (1973).

(5) Mallozzi, P. J., Epstein, H. M., Jung, R. G., Applebaum, D. C., Fairand, B. P., and Gallagher, W. J., "X-Ray Emission from Laser Generated Plasmas", Battelle Report on ARPA Contract DAAH01-71-C-0550 (February 1972).

(6) Mallozzi, P. J., Epstein, H. M., Jung, R. G., and Applebaum, D. C., Patent Application for X-Ray Laser Based on Inner Shell Photoionization by Laser-Plasma X-Rays (1977).

(7) Mallozzi, P. J., Epstein, H. M., Jung, R. G., Applebaum, D. C., Fairand, B. P., Gallagher, W. J., and Campbell, B. E., "A Multi-Kilojoule Short-Pulse Glass Laser and Its Use in High-Temperature Plasma Heating", Proceedings of the Fifth Conference on Plasma Physics and Controlled Thermonuclear Fusion Research (International Atomic Energy Agency), Tokyo, Japan (November 11-15, 1974).

(8) Waynant, R. W., and Elton, R. C., Proc. IEEE, 64 (7) (July 1976).

(9) Mallozzi, P. J., Int. Sch. Quant. Electronics, Erie (June 1973).

(10) Duguay, M. A., Laser Focus, 41-46 (November 1973).

(11) Stankevich, Ya. L., Sov. Phys. Dokl., 15, 356-357 (October 1970).

(12) Elton, R. C., "Quasistationary Population Inversion on Kα Transitions", Appl. Opt., 14, 2243-49 (September 1975).

(13) Stratton, t. F., Plasma Diagnostic Techniques, R. H. Huddlestone and S. L. Leanard, Eds., Chapter 8, Academic Press, New York (1965).

(14) Duguay, M. A., Private Communications.

(15) Madden, R. P., and Codling, K., "Two-Electron Excitation States in Helium", Astrophys. J., 141, 364-75.

(16) Walker, B. C., and Rugge, H. R., "Observation of Autoionizing States in Solar Corona," Astrophysics J., 164, 181-190 (February 15, 1971).

SECTION 2

LASER PRODUCED X-RAY FOR HIGH RESOLUTION LITHOGRAPHY

LASER PRODUCED X-RAY FOR HIGH RESOLUTION LITHOGRAPHY

INTRODUCTION

It is well established that x-ray lithography is an effective means for replicating submicrometer linewidth patterns.[1] Besides replicating test patterns, the technique has been used to fabricate surface acoustic wave devices, bubble domain devices, pn diodes, bipolar transistors, and MOS transistors. The basic concept of x-ray lithography is to use the short wavelength of an x-ray source instead of the long wavelength of an ultraviolet source. This essentially eliminates the diffraction limitation of the ultraviolet source. With this eliminated, x-ray lithography is capable of producing line patterns with a "line width accuracy" of less than 0.1 μm.

The laser-plasma x-ray source has developed into the most intense laboratory x-ray source available in the energy range of ∿ 3/4 to 2 keV. In addition, it appears to be the most attractive laboratory high-average-power x-ray source in the energy range. This energy range is particularly significant for microlithography of integrated circuits. There can be little doubt about the need for high intensity and high-average-power x-ray sources which operate in this energy range, and which are small enough to be used in a laboratory or industrial locations. The rapid growth of synchroton x-ray facilities demonstrates the increasing importance of high-average-power soft x-ray sources. However, the synchrotron is excluded as a laboratory x-ray source because of its size and cost. The commercial applications should expand greatly when the source becomes readily available at the home facility of the user.

In this report the basic phenomenology of the laser plasma x-ray source is studied over an extended range with a rapidly pulsed mode-locked laser system. The use of this quasi-steady state source permitted extensive evaluation of a variety of parameters which have not been studied in detail before. These include the preparation of the initial plasma profile, the main pulse width, and the pulse amplitude. The parameter ranges bridged the regime between steady-state and nonsteady-state models.

References are located on Page 2-23.

To evaluate the plasma phenomonology, it was necessary to investigate several diagnostic techniques not commonly used on laser plasmas. These include rise time scintillator pulse shape analyzers and fast decay component measurements. Also, steady-state calorimetry, spectroscopy, and pin-hole photography were possible because of the quasi-steady-state nature of the source.

Because the high repetition rate laser-plasma x-ray source is a new concept, a large portion of the program was necessarily devoted to developing the technique, troubleshooting problems, and optimizing the source. These included optimizing the rotation rate of the target; devising systems to prevent the lens from being destroyed by focused reflections when a small amount of target blowoff negated the antireflection coating on one side of the lens; and maintaining consistent output from the mode locked laser. One of the main conclusions of this study is that these problems can be overcome and that this type of soft x-ray source is very valuable for research and ultimately for commercial lithography.

The laser targets which comprised the x-ray source were 2.5 cm diameter by 2.0 cm long, yielding an area of 15.2 cm^2. Since the laser focal spot size can be less than 50 μm, over one half million pulses might be obtained from a single target. Actually the screw drive in our system was a standard micrometer with about 625 μm advance per turn. This limits the possible target life to approximately 50,000 pulses. As shown in Figure 2-1, the x-ray yield does not decrease significantly until the spacing between pulses is less than about 70 μm. On the order of 50,000 pulses per target can be obtained from the present system, and this can be extended to about 500,000 pulses with a finer screw drive. The life of the target can easily be extended to equal the life of the laser flash lamps by using bigger cylinders. The flash lamps of the Quantel laser employed for the present experiment have a rated life of approximately 1,000,000 flashes.

The second problem associated with a repetitively pulsed laser is that the vaporized target material eventually builds up a thin reflecting coating on the lens, which defeats the antireflection coating. This deposited layer is thin enough that the energy loss is essentially negligible for one target lifetime. However, the small amount of reflected light can be multiply reflected to a focus in the lens, causing progressive damage. This problem

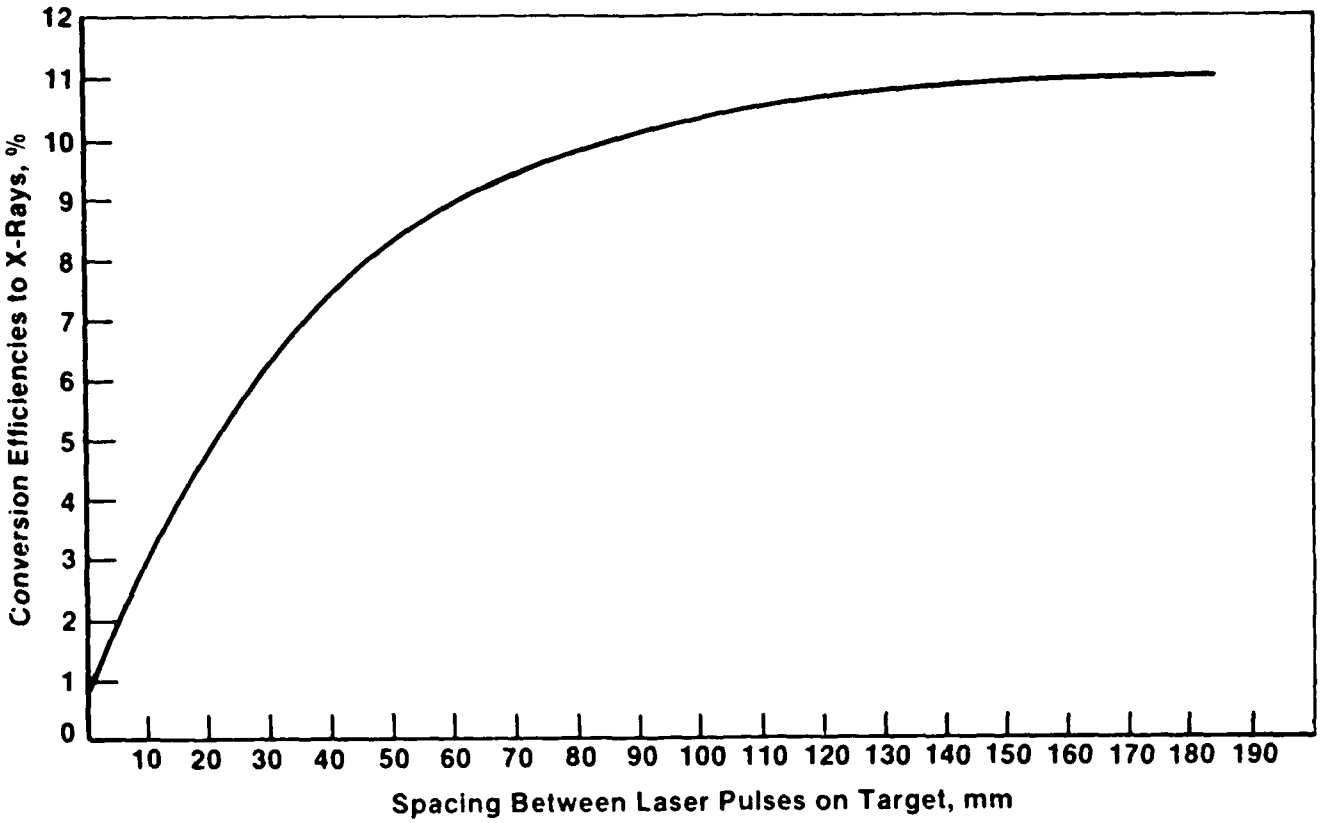

FIGURE 2-1. EFFECT OF FOCAL SPOT SPACING ON X-RAY CONVERSION EFFICIENCY

was solved by expanding the beam by about a factor of five and using a lens with an equivalent f number but a factor of five further away. A hole was drilled in the center of the lens to eliminate multiple reflective focusing at the center. Since brightness is conserved in this change, the size of the focal spot is the same, and the x-ray generation is unaffected.

Diagnostic Techniques

The principal diagnostic techniques are crystal diffraction spectroscopy, steady-state calorimetry, and pulse width measurements. Spectra were taken with a flat KAP crystal. Since the quasi-steady-state spectroscopy differed from the single pulse experiments only in the photon statistics, no further discussion of this technique is needed.

Single pulse x-ray calorimetry is usually done with pyroelectric detectors. These have some inherent uncertainties in this type of application because of the sensitivity of this type of detector to mechanical vibrations or small shocks. The pure calorimetric detector applicable to the quasi-steady state or high repetition rate experiments is inherently more accurate and more stable. The principle precaution that must be taken with the steady state calorimeter is to make certain that the debris heat doesn't register in the calorimeter.

Two distinct experimental techniques were compared in the time dependent diagnostics of the x-ray pulse. Both methods have a time resolution capability limited by the detector to 9×10^{-11} seconds. The detector was a Hamamatsu photodiode. The first method is based on the fast rise time characteristics of unitary crystals. If a scintillator could be found with a perfectly sharp rise and a very long decay time, the pulse shape of the emitted light would simply represent the time integrated x-ray flux, and a time resolved pulse would be obtained by differentiating the corrected intensity profile. In practice, the fast rise is attainable, but the long decay is elusive. The rise time of organic crystals in general is a function of the concentration of the fluorescent solute.[2] Since time is required for energy deposited in the solvent to diffuse to active solute, the major emitted component of the binary or tertiary, liquid or plastic scintillator should have a rise time too long for subnanosecond resoltuion. Of course,

a small component of the x-ray energy will be deposited directly in the solute, producing a weak signal of very fast rise time. The use of this signal will be discussed in the second method.

In any case a logical alternative to the binary or tertiary detector is to use a unitary fluorescent material. The rise time is limited only by the equilibration time of the incident x-ray energy for unitary organic crystals such as anthracene or stilbene. This time is of the order of picoseconds for the low energy x-rays of interest here. The x-rays are absorbed by the photoelectric effect and the emitted electrons slow down in about 10^{-12} seconds raising the molecules of the scintillator to upper level excited electronic states. These states decay in about 10^{-12} seconds by internal conversion, primarily to the lowest excited singlet state($^1X^*$), which decays by radiative emission producing the fast component of the visible scintillator output.[3] A slower component of the scintillator emission arises from the excited triplet state ($^3X^*$). The delayed emission is due to bimolecular association of $^3X^*$

$$^3X^* + {}^3X^* \rightarrow {}^1X^* + {}^1X$$

The decay rate of this slow component is not exponential and is dependent on the density of excitation.[4] Thus, a strongly ionizing charged heavy particle will exhibit a different decay time in the slow component than an x-ray or an electron, giving rise to the decay time discrimination technique often used to distinguish neutrons from gammas. This slow (typically 30 nanoseconds) component is erroneously quoted in handbooks as the fluorescent decay time of anthracene. However, in the subnanosecond regime, the contribution of the slow component to the scintillator output is unimportant and the fast component dominates. The time constant of the fast component is 1 nanosecond.

A 1-nanosecond decay time constant is hardly long, in the present experiments, but a correction for the decay can easily be applied to the differentiated curve, so that this is not a serious drawback to the technique. The light emission, E(t), from the scintillator at time,t, caused by the time-dependent x-ray fluence, S(t), is

$$E(t) = C\int_o^t dt' \, S(t') \exp-(t-t')/\tau \quad , \tag{2-1}$$

where τ is the decay time of the scintillator. Differentiating Equation (2-1) gives

$$d/dt[E(t)] = C[S(t) - \frac{1}{\tau}\int_o^t dt' S(t') \exp-(t-t')/\tau] \quad , \tag{2-2}$$

and substituting Equation (2-1) into (2-1),

$$S(t) = 1/C \{d/dt[E(t)] + E(t)/\tau\} \quad . \tag{2-3}$$

Equation (2-3) shows that a finite decay constant simply requires the addition of $E(t)/\tau$ to the derivative. It would certainly be preferable if a fast rise time scintillator were available with a longer decay time. However, the short decay constant and high scintillation efficiency of anthracene are advantageous where low x-ray intensities limit the accuracy of the measurements.

The second method for time dependent diagnostics is based on a characteristic of plastic scintillation observed by M. Dugay[5]. As mentioned earlier a fraction of the soft x-ray radiation in an organic scintillator is absorbed directly by the fluorescent solute, producing a very fast rise time component. Dugay observed that there is also a very fast time decay component in plastic scintillators. It is, therefore, possible to measure shapes of pulses which are short compared to the several nanosecond dominant time constant.

The x-rays passed through a 1/2 mil Be filter before entering the scintillator. The Be filter blocked out the laser pulse and the plasma light. The scintillor emissions were transmitted through a light pipe and into the photo diode after passing through an interference filter designed to remove any 1.06 μm laser light which might have leaked through pin holes in the Be. The x-ray output is almost the same as the laser pulse shape as shown in Figure 2-2.

Experimental Program

The experimental program primarily involved x-ray measurements over an extensive parameter matrix. The diagnostic methods discussed in the previous section along with those methods applied in previous years

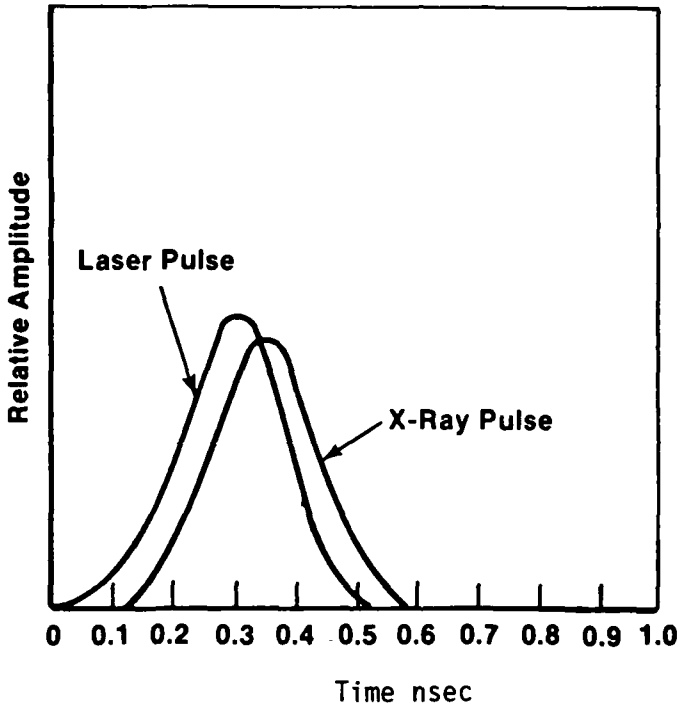

FIGURE 2-2. COMPARISON OF LASER PULSE WITH X-RAY PULSE

of this program were applied to a wide range of laser plasma conditions. Specifically, the parameters varied in this study were (1) laser pulse energy, (2) laser pulse width, (3) plasma profile, (4) laser wavelength, (5) target atomic number, (6) initial focal area, and (7) focal ratio of the lens. The laser pulse energy was varied from 0 to .3j, although the upper limit of the pulse energy was not available for the shortest pulse widths. Three laser pulse widths were used, 300 psec, 180 psec, and 30 psec. The majority of the study was done at a wavelength of 1.06 μm. However, a limited study at 0.53 μm was completed. The plasma profile was modified over a wide range by varying the leakage foot through the pulse selector pockels cell. A wide variety of targets including Cu, Fe, Cr, Ti, V, Nb, Al, Mg, F, and W were included, but the majority of the parameter studies were done with Cu and Al. Only two lens focal ratios were employed.

Figure 2-3 shows the x-ray output efficiency over 1 keV for the 300, 180, and 30 psec pulses. In the scaling section we show that x-ray production efficiency reaches a maximum when the laser power is given by

$$P_L \gtrsim 10^{14} \pi v_\tau D_B \Delta \qquad (2\text{-}4)$$

where v is the average velocity of the expanding critical density front. For copper this is about 10^7 cm/sec. If the laser were diffraction limited, the beam divergence Δ would be $1.2\lambda/D_B$, where D_B is the beam diameter. Due to pumping stress induced distortions, the value of $D_B\Delta$ is 10^{-3} instead of 10^{-4}. For the .3 nsec pulse width, τ, the required laser pulse energy for efficient x-ray production is 0.6j. Only 0.3 j/pulse was available and losses in the optics decreased this by about 10 percent. As can be seen from Figure 2-3, the x-ray conversion efficiency for the 0.3 nsec pulse width is very low, and the efficiency drops off rapidly with decreasing energy for the .18 nsec pulse width below the value specified by Equation 2-4. As expected, considerably higher powers do not produce greater x-ray conversion efficiencies.

As long as the laser power is safely above the level specified by Equation 2-4, the x-ray conversion efficiency is essentially independent of pulse width until it begins to fall off at the shortest pulse widths of ~30 psec. The loss of efficiency at the shortest pulse width is probably due to the fact that the residency time of the ions in the heated region of the plasma is not sufficient to allow the ionization to approach steady state.

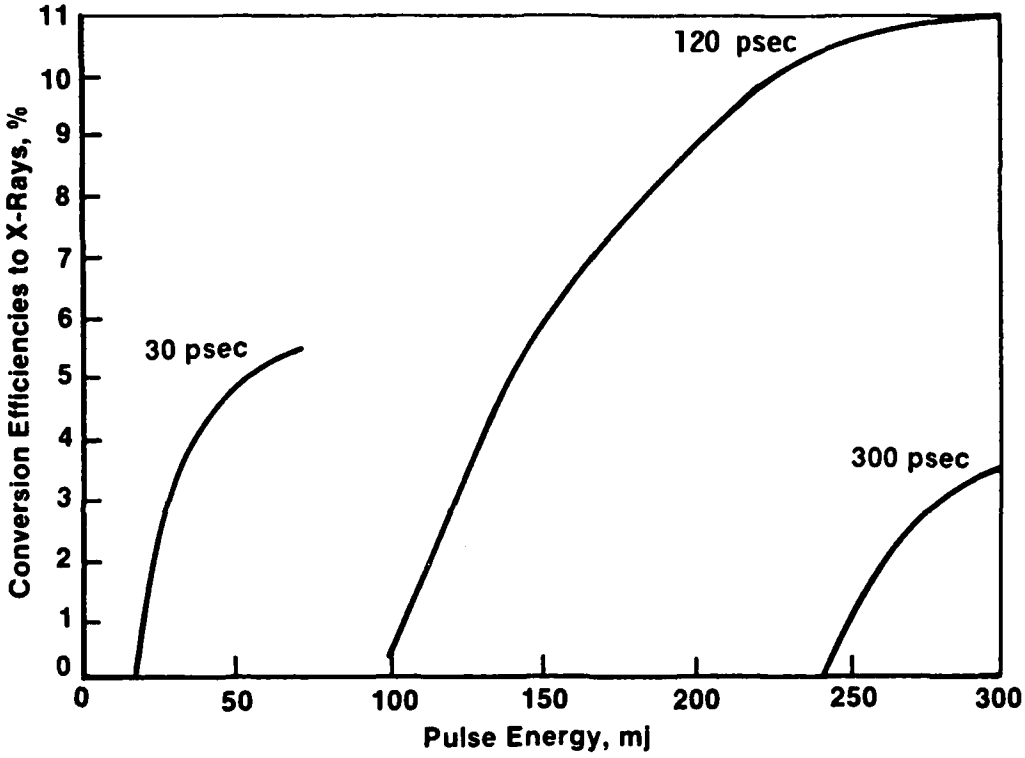

FIGURE 2-3. OUTPUT EFFICIENCY FOR X-RAYS OVER 1 keV

The effect of a low level of laser energy on the target before the main pulse is to prepare a plasma profile. This is accomplished by slightly opening the pockels cell on the pulse slicer. The calculated characteristic of this plasma foot are shown in the following equations:

$$T_\infty \approx \sigma^{-1/4} I_f^{1/4} \tag{2-5}$$

$$d \approx \left[\frac{(Z_\infty + 1)K}{M}\right]^{1/2} \sigma^{-1/8} I_f^{1/8} \tau_f \tag{2-6}$$

$$(n_i)_a \approx \frac{M^{1/2} \sigma^{3/8} I_f^{5/8}}{6(Z_\infty + 1)^{3/2} k^{3/2}} \tag{2-7}$$

where I_f is the foot intensity, σ is the Stefan-Boltzman constant, M is the ion mass, T_∞, Z^*_∞ are the assymptotic values of the temperature and mean ion effective charge respectively, τ_f is the pulse width of the laser foot, d is the foot-plasma thickness, and k is the Boltzman constant.

Although the leakage pulse has a series of mode locked spikes, the effective profile can be estimated by averaging over the spikes. As can be seen from Figure 2-4 the conversion efficiency is relatively insensitive to the amount of leakage foot over a very wide range for the more energetic main pulse. However, as the energy of the main pulse decreases, the effect of the foot becomes much more critical. this study was done only for the .18 nsec pulse width.

In addition to the experiments at 1.06 μm, a limited number of experiments were also conducted with a frequency doubled beam at 0.53 μm. The effect of laser foot on efficiency was the same for 0.53 μm as for 1.06 within the experimental accuracy. The x-ray spectrum and conversion efficiencies for the L-line x-rays are also the same for these two wavelengths. The k-line x-rays differ substantially for the 0.53 μm wavelength compared to the 1.06 μm. These differences are discussed under previous research results.

A variety of elements in the K and L-line emission regimes were investigated. The low atomic number elements were of particular interest because their spectra are required for the design of the x-ray pumped photoemission x-ray laser experiments planned for 1985. These elements include Al, Mg, Na, F, and C. Spectra for some of these elements are shown

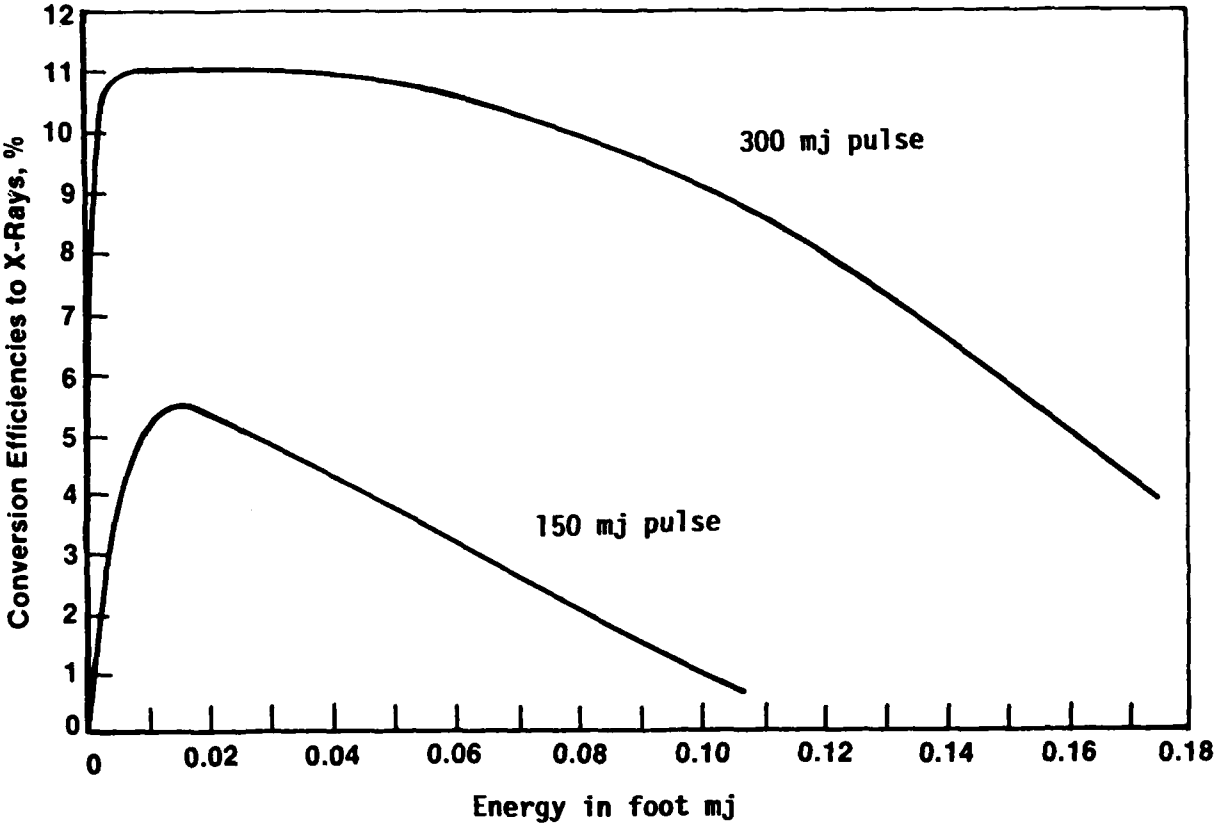

FIGURE 2-4. EFFECT OF PREPULSE ON X-RAY EFFICIENCY

in Figure 2-5. For Al and Mg the He-like resonance lines dominate, while for the lower atomic number element, such as F, the H-like lines dominate. This effect is shown in Figures 2-6 and 2-11.

The absorption of the emitted x-rays by the plasma is also of interest for computer modeling. Table 2-1 shows the ratio of the intensity of a number of lines measured near tangential to the target surface to the intensity of the same lines measured normal to the surface. Self-absorption of the line within the plasma gives a ratio less than one. Amplification, as with an x-ray laser, would give a ratio greater than one. As can be seen from Table 2-1, the line ratios are approximately 1 within experimental error. A second method to experimentally evaluate self absorption is to examine line profiles for self absorption dips in the center of the line. The absorption line width will be narrower than the emission width because Stark and Doppler broadening are lower in the colder less dense regions of the plasma. If stimulated absorption occurs, the absorption will be intensity dependent and the absorption line width will narrow during transport through the plasma.

TABLE 2-1. RATIO OF TANGENTIAL TO NORMAL INTENSITIES

Line	AL						
	1	2	3	4	5	6	8
R	1.05	1.02	.96	.94	.98	1.08	.94
Line	F						
R	.99	1.04	1.00	.95	.97	.94	1.03

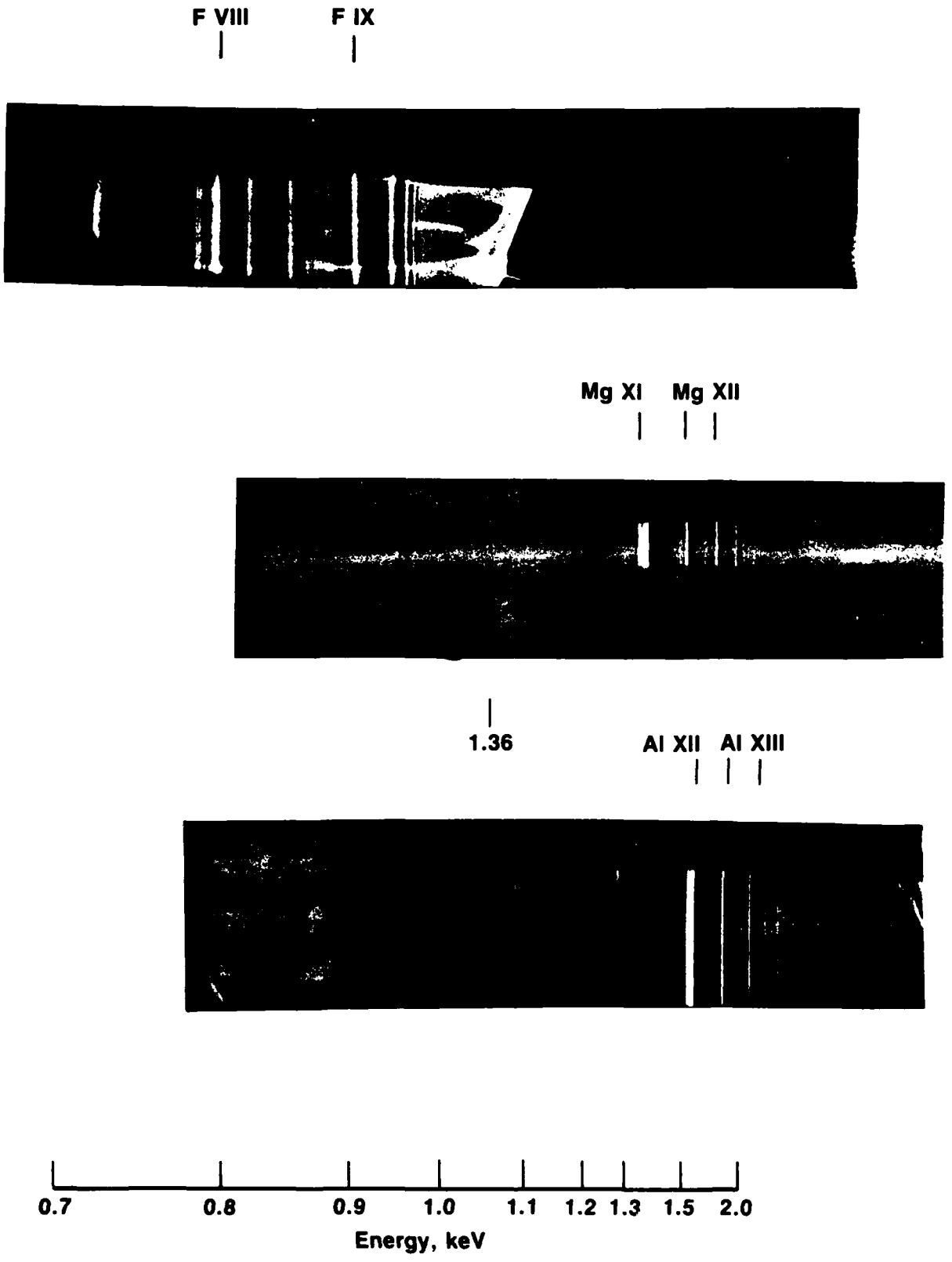

FIGURE 2-5. K-LINE SPECTRA

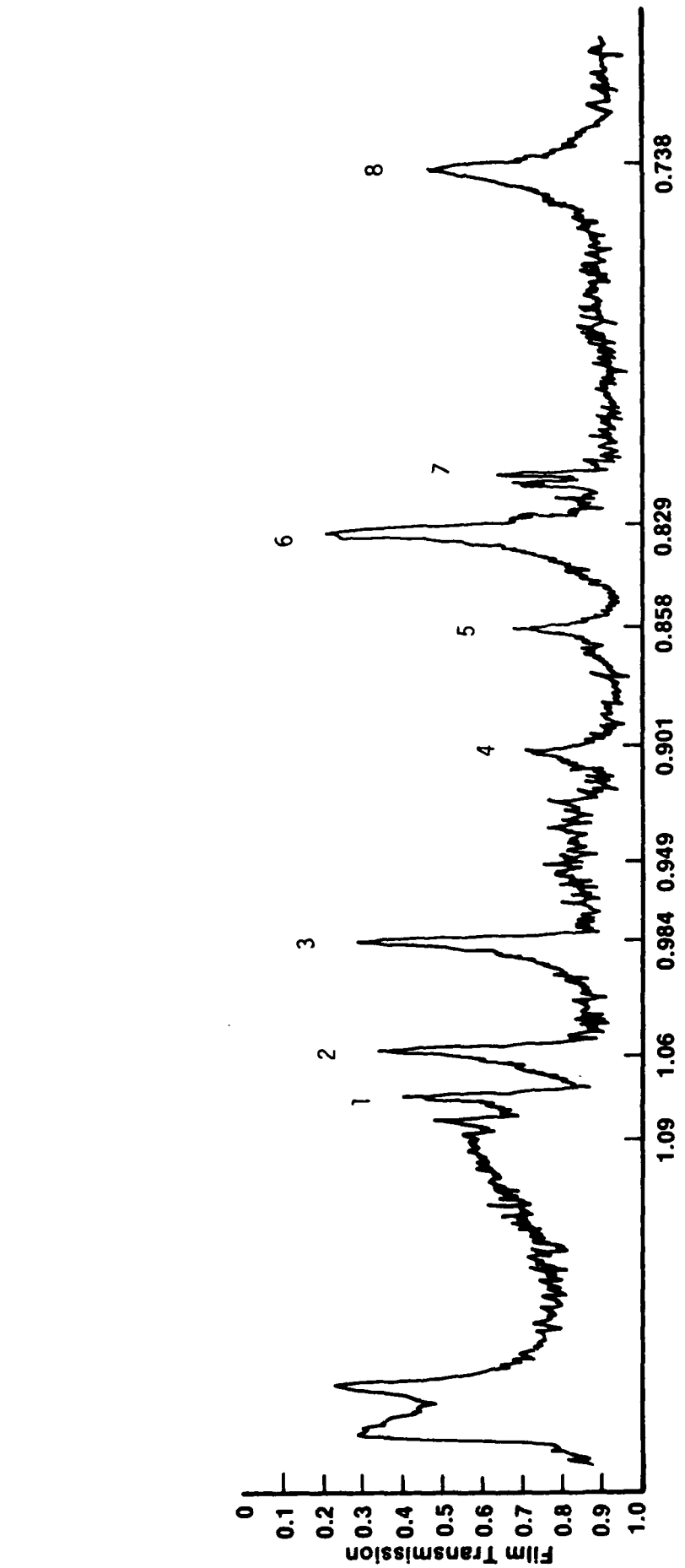

FIGURE 2-6. DENSITOMETER TRACE OF F X-RAY SPECTRUM

Single shot ∿100J laser pulses were used for absorption studies to give larger plasmas (∿150 μm) and emphasize absorption. For the line profile studies the x-rays were dispered by or flat KAP crystal and the x-ray spectrum was recorded on type M films. The resolution obtainable in these experiments was calculated to be leV. Any absorption depression in the line profile should have been resolved in these experiments. None was seen. It is probable that the Doppler broadening associated with the time integrated measurement through an expanding plasma with changing velocity smeared out the line profiles.

The L-line emitters are of greater significance as x-ray source for lithography of printed circuits. The L-line emitters which were studied include Cu, Fe, Cr, Ti, V, and Nb. The Ti and Nb represent the approximate upper and lower ends of the L-band of lines. With Ti, the strongest L-resonances lines are about 1/2 keV and very little L-line energy is above 1 keV. With Nb, the strongest resonance lines are at almost 2 keV, and are an order of magnitude weaker than the strongest resonance lines of Fe. In general we can see that ∿Cu will be the most efficient target for L-line radiation in the 1-1.5 keV energy band. Actually, the L-band for Cu starts with the large resonance lines at 0.95 and 0.98 keV. Probably Zn or Ga would be a little better in this energy band, but the surfaces are less suitable as laser targets and probably allow more depopulation of the amplifier by back reflection. Nd is an example of an element whose lowest lying L-resonance line of 1.86 keV is so high in energy that it is only weakly excited. (Figures 2-7, 2-8, and 2-10)

The M-line peak is of only marginal interest for x-ray lithography because it is an efficient producer only of very soft x-rays, on the order of a few hundred eV. Those elements such as W, whose M-lines are of an energy high enough to be interesting, are far on the wing of the efficiency peak.

The initial focal area was varied over a range of about an order of magnitude by changing the position of the target in the focal cone. These experiments were performed only with the Cu target, and the results are shown in Figure 2-9. Within the range of parameters evaluated, the change in focal area had almost the same effect on efficiency as the change in power density at a fixed focal area. This would indicate that most of the

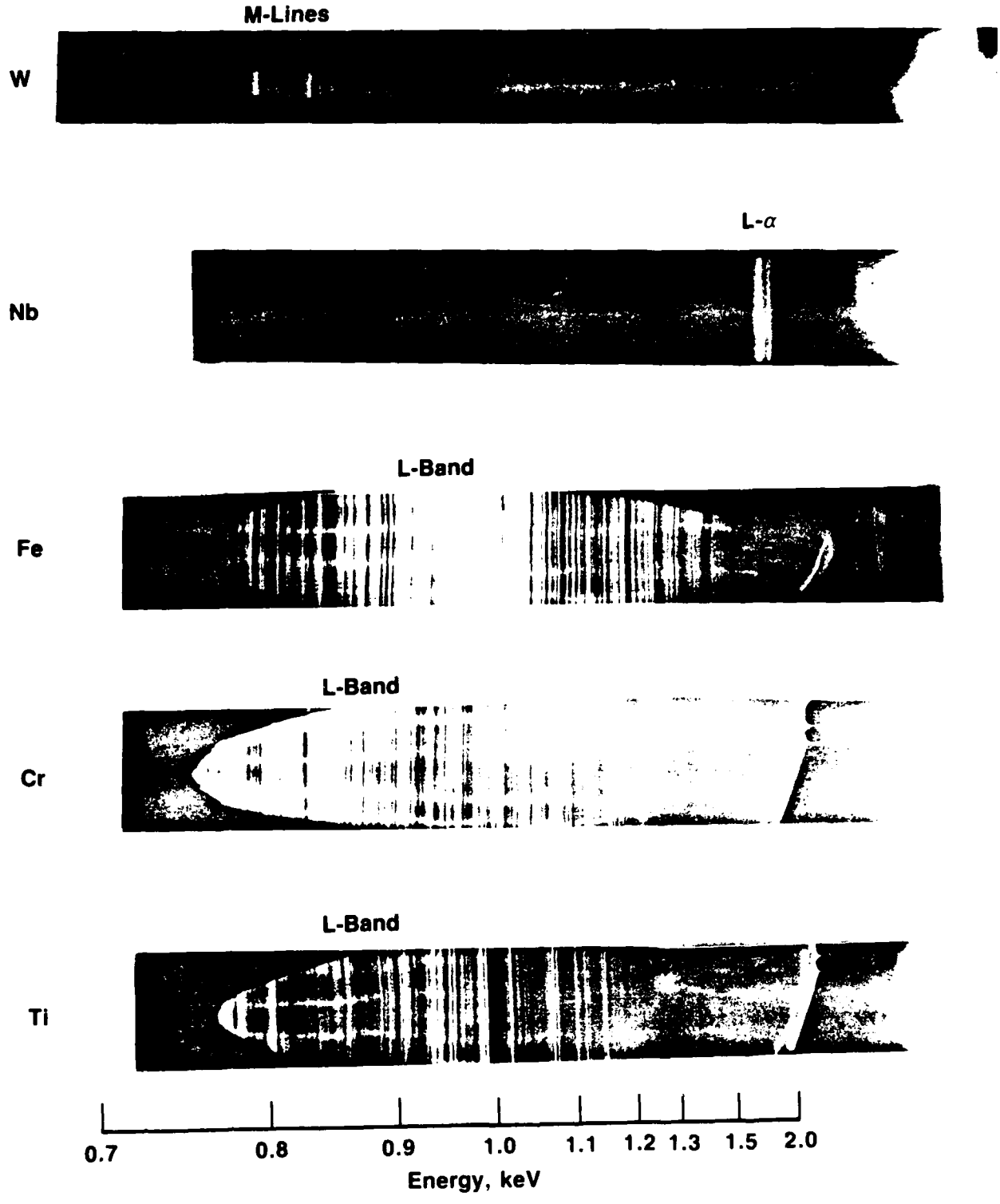

FIGURE 2-7. L AND M-LINE SPECTRA

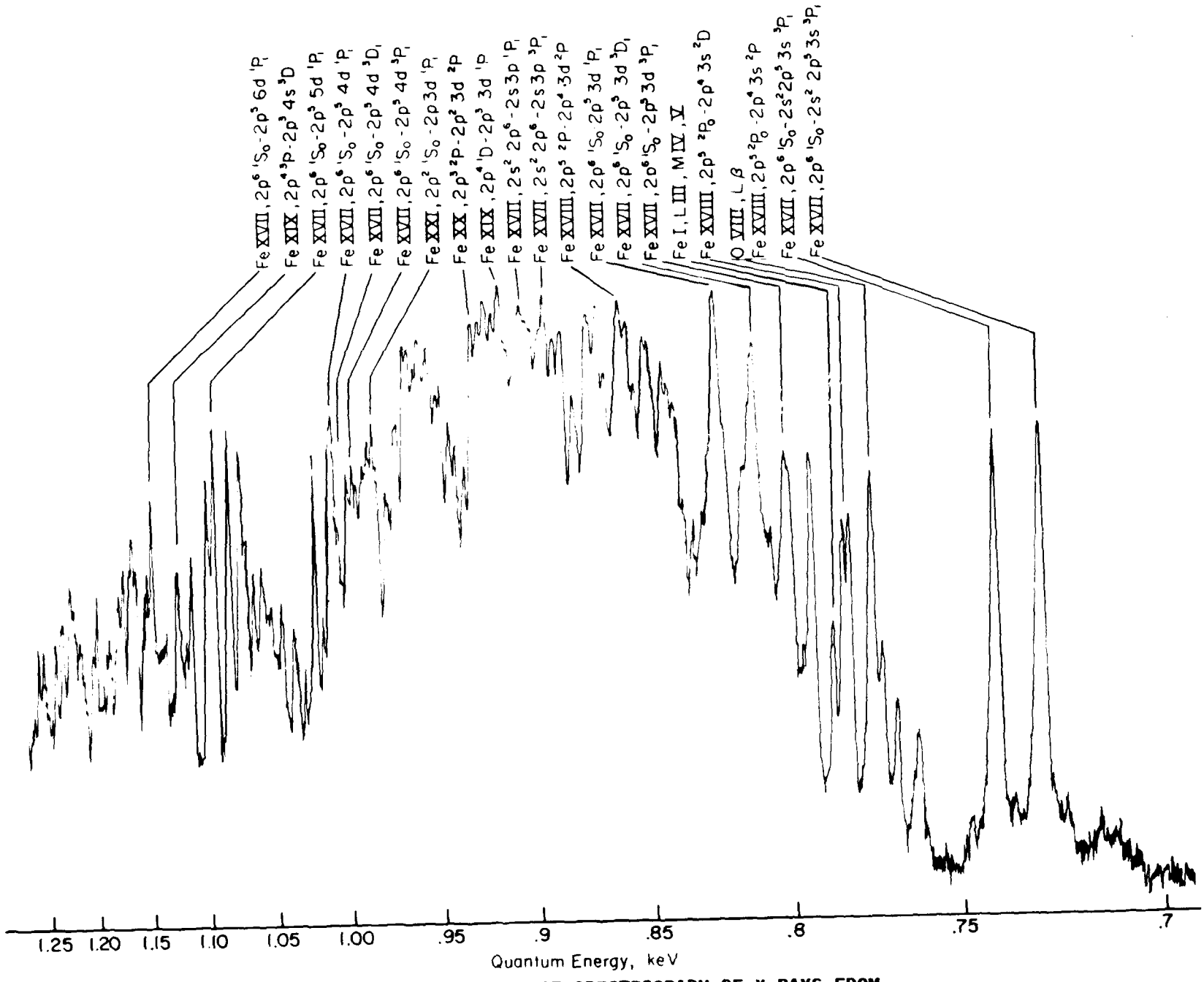

FIGURE 2-8. DENSITOMETER TRACING OF SPECTROGRAPH OF X-RAYS FROM IRON SLAB TARGET USING BENT CRYSTAL SPECTROMETER
(Laser flux is incident on iron slab at $\sim 10^{14}$ watts/cm^2)

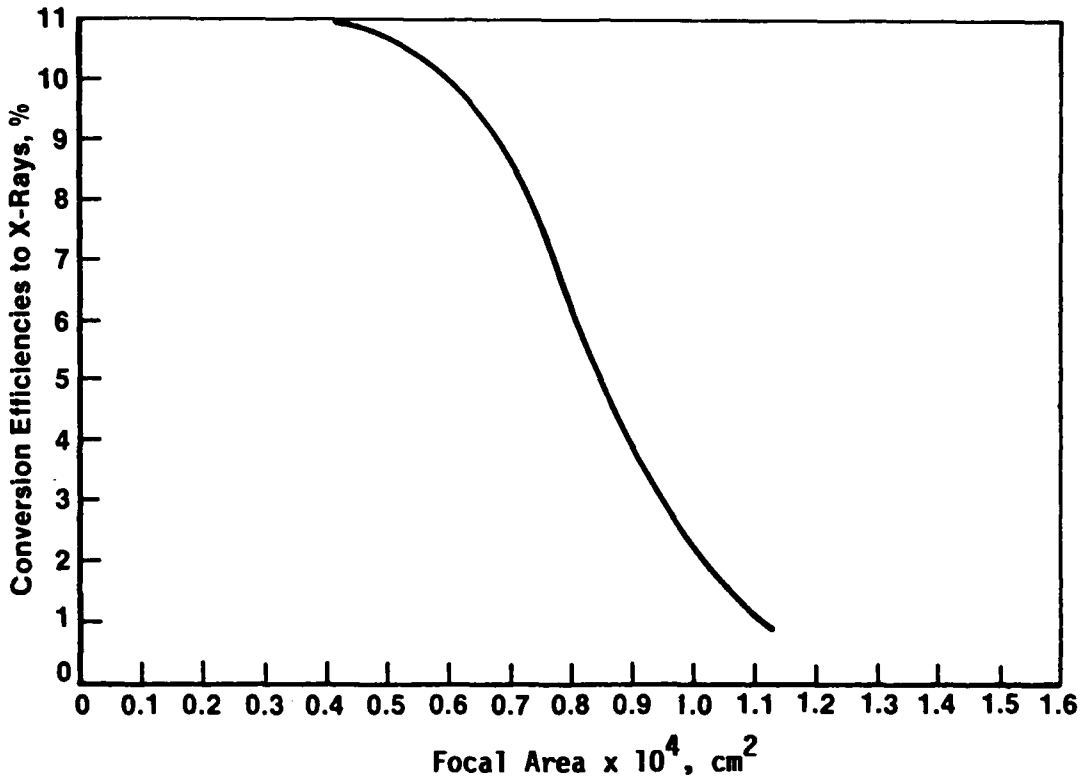

FIGURE 2-9. EFFECT OF FOCAL AREA ON X-RAY EFFICIENCY FOR 300 mj, 0.18 msec LASER PULSES

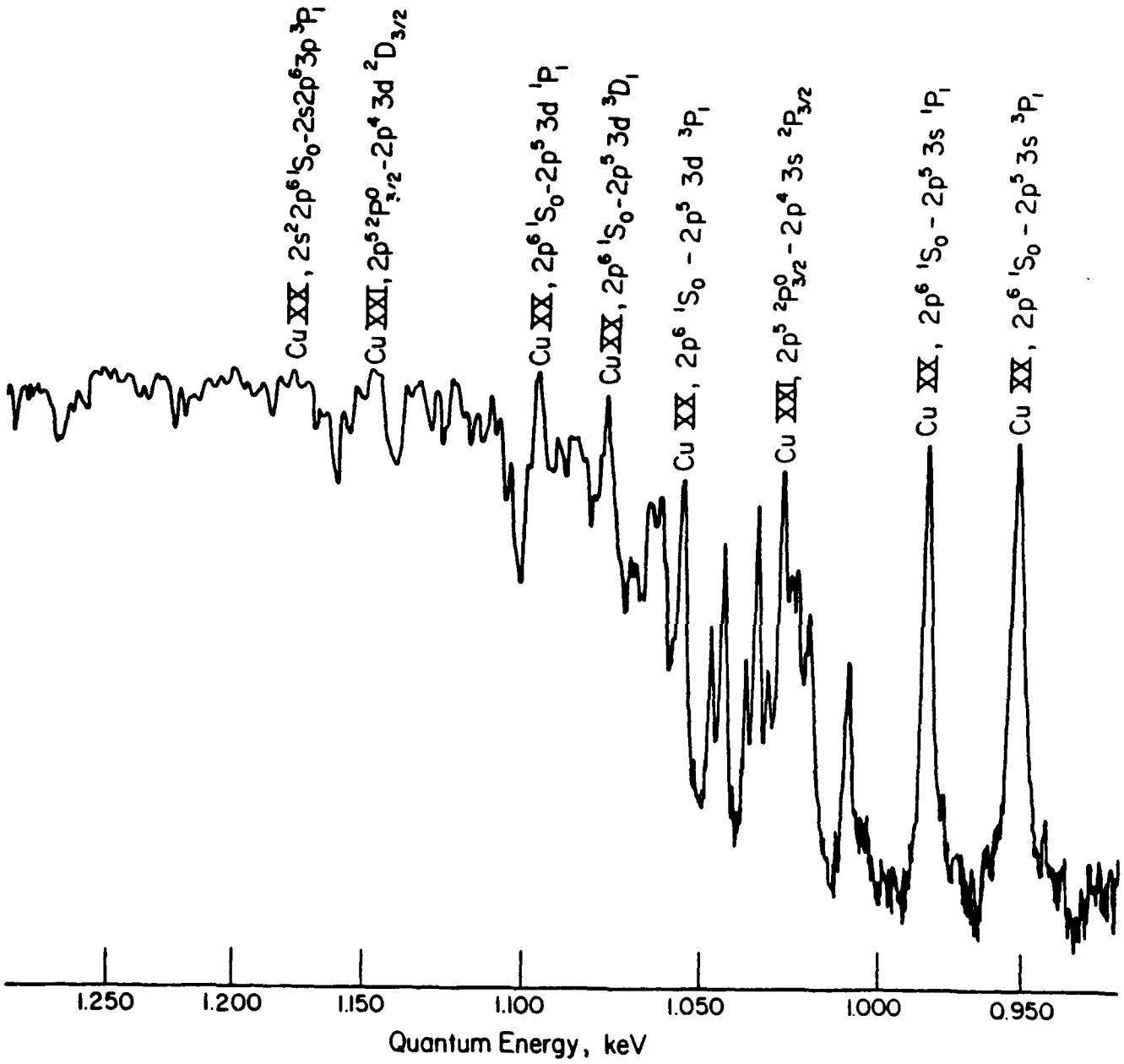

FIGURE 2-10. DENSITOMETER TRACING OF BENT CRYSTAL SPECTROGRAPH OF X-RAYS PRODUCED FROM COPPER TARGET WITH NEODYMIUM LASER PULSE

radiation is emitted while the geometry is still essentially planar. As shown in the computer printout of Figure A-7, the critical density plane has moved only about 10 μm in 135 psec. This motion is small compared with the diameter of the focal spot.

Only two focal ratios were used in these experiments, f/13 and f/4.5. With the f/4.5 lens, the focal spot diameter was determined by the quality of the lens instead of the quality of the beam. The focal spot diameter for the f/13 lens was ∿100 μm. For the f/4.5 lens, the focal diameter was ∿70 μm. The conversion efficiency for the f/4.5 lens is approximately 1.5 times that for the f/13 lens in tests with 0.3j laser pulse of 180 psec pulse width. The optimum f number[6] is given by

$$f_{opt} = \left(\frac{v\,\tau}{D_B\,\Delta}\right)^{1/2}$$

Thus, the optimum f number for this system would have been ∿f/1, and it is expected that the smaller f number lens yields better conversion efficiency. If the laser were diffraction limited, the optimum f number would increase to 3.3 and the f/4.5 lens would be much better matched.

Scaling Criteria

For the high-average power applications, it is advantageous to use a low pulse energy, high repetition rate laser. The high conversion rates of laser energy to x-rays (up to 27 percent over 300 eV) at Battelle have been achieved in the near steady-state coronal plasma radiation regime with carefully pre-conditioned plasma profiles. The rule of thumb dividing line between steady state and time dependent coronal plasmas is given by $t \simeq 10^{12}/n_e$. Since the critical plasma density where the principal absorption occurs is

$n_e \approx 10^{21}$, radiation times greater than 1 nanosecond can be reasonably assumed to be steady state, if the plasma remains in the dense region for 1 nanosecond. This is an important factor if we are to assume, for scaling purposes, that the radiated x-ray spectrum depends only on the power density and electron density gradient at the critical-density surface. If quasi-steady state conditions have not been achieved, the spectrum will depend on previous irradiation history.

The focal diameter, D_f, at the critical surface of the plasma changes as the plasma moves out at a velocity v. If the laser is focused on the critical density surface at time t, D_f is given by

$$D_f = f\, D_B \Delta + v|t|f \tag{2-8}$$

where f is the f number of a perfect lens, D_B is the incoming beam diameter, Δ is the natural beam divergence, and v is the plasma velocity. The first term represents the initial focal diameter on the critical surface and the second is the increase in diameter due to the expanding plasma. The situation in which the laser is focused at the position which the critical density surface will occupy when the laser reaches peak power corresponds to t = 0 when the laser power is at its maximum. However, for purposes of scaling, this is not a factor.

The power density at focus, P, is given by

$$P = 4/\pi[f^2 D_B{}^2 \Delta^2/P_L + 2v|t|D_B\Delta/P_L + v^2t^2/(f^2P_L)]^{-1} \tag{2-9}$$

where P_L is the laser pulse power. In the steady state, v is a function only of P for a given target. If f and Δ are kept constant and t and D_B are scaled as $P_L{}^{1/2}$, P will remain unaffected. Thus, the spectrum and conversion efficiency will be conserved with this scaling. This type of scaling has been tested at Battelle over a laser pulse energy range of over 100, and found to be valid.

The optimum f number for the lens is given by

$$f_{opt} = \left(\frac{vt}{D_B\Delta}\right)^{1/2} \tag{2-10}$$

Of course, the f number of the lens cannot change with time on a nanosecond time scale. For a high average power system we would like to have P exceed a threshold for an extended time rather than have the peak power coincide with the minimum focal diameter. This also keeps v relatively constant through a large part of the pulse. Plasma velocity is a weak function of P anyway. Choosing the lens to optimize the power at time τ gives

$$P = \frac{P_L}{\pi v \tau D_B \Delta} \qquad (2\text{-}11)$$

In scaling, τ is proportional to the pulsewidth.

If high conversion efficiency is desired for low energy pulses, a short pulse width is required. However, it is not obvious why low energy pulses are desirable for a high average power laser source. Large pulse, solid state lasers are almost universally made of glass. Because of the thermal expansion and low pumping efficiency of glass, it is several times more expensive to obtain the same average power from a glass system than a YAG system. Unfortunately YAG rods are limited to small diameters (1 cm or less for commercial systems). It is, therefore, advantageous to be able to operate with low energy pulses. Since our past experience has shown that P should exceed $\sim 2 \times 10^{13}$ W/cm^2, a pulse energy under 1 joule requires a pulse width less than 1 nanosecond. Such pulse width can only be attained on commercial systems by mode locking. At this pulse width the $\sim$ 1 cm diameter YAG rod is limited to 0.3 - 0.4 joules per pulse if long life is required.

REFERENCES

(1) Smith, H. I., and Flanders, D. C., Japanese J. Appl. Phys., 16, Suppl. 16-1, 61-65 (1977).

(2) Nuttleman, R. H., Epstein, H. M., Beal, J. W., and Mallozzi, P. J., in Advances in x-RAY ANALYSIS, Eds. W. L. Pickles, C. S. Barrett, J. B. Newkirk, and C. O. Raad, 18, Plenum Press, New York (1975).

(3) Windsor, M. W., in Physics and Chemistry of the Organic Solid State", Eds. D. Fox, M. M. Lobes, and A. Weissberger, Vol. II, Interscience (1965).

(4) Laustriat, G., in Organic Scintillators", Ed. Horrocks, D. L., Gordon and Breach (1966).

(5) Dugay, M. A., and Olsen, J. N., IEEE J. Quant. Elect., 170-72 (April, 1979).

(6) Mallozzi, P. J., Epstein, H. M., Jung, R. G., Applebaum, D. C., Fairand, B. P., and Gallagher, W. J., "X-Ray Emission from Laser Generated Plasmas", Battelle Report on ARPA Contract DAAH01-71-C-0550 (February, 1972).

(7) Epstein, H. M., in Material Processing Symposium", Ed. Metzbower, E. A., ICALEO, LIA, Vol. 38 (1984).

(8) Boiko, V. A., Piluz, S. A., and Safronova, U. I., "The Analysis of Satellites to the H-Like Ion Resonance Lines Observed in the X-Ray Region, Mon. Not. R. Astr. Soc., 118, 107-120 (1978).

(9) Bhalla, C. P., Gabriel, A. H., and Presnyakov, L. P., Mon. Not. R. Astr. Soc., 172, 359 (1975).

(10) Stratton, T. F., Plasma Diagnostic Techniques, R. H. Huddlestine and S. L. Leonard, Eds., Chapter 8, Academic Press, New York (1965).

APPENDIX A

SINGLE LASER PULSE X-RAY GENERATION

APPENDIX A

SINGLE LASER PULSE X-RAY GENERATION

INTRODUCTION

These experiments have concentrated on the effect of wavelength and intensity on the excitation of K and L levels. The targets and the regimes of laser pulse parameters were chosen to provide large time dependent corona effects. Most laser plasma x-ray experimental studies have been conducted with laser pulse parameters in a regime where the variation in the laser output causes no more than a linear change in the x-ray output. Applications require a reproducible and predictable x-ray source. However, the best insight into the mechanism of the time dependent corona model can be obtained in experiments where the transitions under observation are far from steady state.

Several general conclusions can be drawn so far from this study. First, the temperature of the plasma contributing to the radiation is very weakly dependent on wavelength. It is also weakly dependent on intensity except at low intensities. Second, at low laser intensities, the x-ray emission from K-level transitions in Al is approximately proportional to the square of the laser frequency. Third, the x-ray emission from L-level transitions in Cu is almost independent of laser frequency. Fourth, at low laser irradiation levels, the x-ray emission decreases exponentially with intensity. These four observations should be explainable on the basis of a one-dimensional laser-plasma model. A fifth observation, that the electron temperature is cooler for an Al target than for a copper target, requires a two-dimensional analysis.

The system's implications of the laser-plasma x-ray source are discussed in the LIA article in Appendix B.

DISCUSSIONS

Since the plasmas are usually not in a steady state and since the plasma electron temperature varies in both space and time, some discussion of the plasma temperatures derived from x-ray measurements is in order. Any determination of temperature by comparisons of ratios of lines from different ionization states is very questionable. Temperature determinations from the intensity ratio of satellite to resonance lines in the same ionization state are more justifiable. Satellites of the He- and H-like ions have been evaluated for several elements.[1,2] The temperature results from the H-like measurements should be acceptable in the time dependent corona regime because the populations in the upper level are produced dominantly by dielectronic recombination. (In the excitation of the He-like satellites, excitation from the inner shell of the corresponding Li-like ions plays a major role.)[2]

The temperature is most often derived from the measured shape of the continuum radiation. That radiation can be of two types: plasma bremsstrahlung, E_{ff} and recombination radiation, E_{fb}

$$\frac{dE_{ff}}{d\nu} \sim \Sigma\, n_e n_i\, Z_i^2\, \frac{\exp(h\nu/kT_e)}{(kT_e)^{1/2}}$$

$$\frac{dE_{fb}}{d\nu} \sim n_e\, n_{i+1}\, Z_i^4\, \frac{\exp[-h\nu-\chi_{i,n})/kT_e]}{(kT_e)^{3/2}}$$

Because of the Z^4 dependence in the recombination radiation, this type of continuum will dominate for low kT_e. In fact, the plasma bremsstrahlung radiation will not equal the recombination radiation until

$$kT_e > 3\chi_H Z^2$$

where χ_H is the energy of the hydrogen-like state.

The temperature can be directly derived from differential absorption measurement by evaluating the integral

$$\frac{I}{I_o} = \int_{\chi_i}^{\infty} \exp\,(\chi_i - h\nu)/kT_e \exp[-\Sigma(h\nu t)]\, d\,(h\nu)$$

where $\frac{I}{I_o}$ is the attenuation through a foil of thickness, t, and mass absorption cross section, $\Sigma(h\nu)$. For Be, in this range of interest

$$\Sigma(h\nu) \sim 570(h\nu)^{-3}$$

where $(h\nu)$ is in keV.

The principal x-ray emissions in the Al target experiments were He-like K lines and recombination radiation (Figure A-1). Figure A-2 shows the transmitted intensities as a function of Be absorber thickness for Al targets irradiated with 0.53 μm and 1.06 μm laser pulse 1.5 nanosecond in width. It can be seen that for low intensities the x-ray intensity is dominated by the He-like Al line (the $1S^2$ - 1S3 p transitions including satellites). As the intensity increases, the H-like Al line (1S3 p transition including satellites) becomes noticeable but not dominant. Finally at powers exceeding 5×10^{13} with the .53 μm wavelength, the recombination radiation becomes dominant. The plasma electron temperature as determined from the slope of the absorption curve in the recombination regime is very weakly dependent on wavelength and is ∼ 600 eV for both the 1.06 and .53 μm wavelengths at 5×10^{13} w/cm^2.

Several interesting aspects of the laser-plasma phenomonology are evident from Figure A-2. The Al targets irradiated with 1.06 μm laser light emitted dominantly He-like line radiation with recombination radiation representing a few percent of the total. This is true even at power densities of 10^{14} w/cm^2. However, the Al target irradiated with 0.53 μm laser light showed almost as much H-like as He-like Al emissions and the percentage of recombination radiation was about double the intensity for the same power level as the 1.06 μm tests. When the power is increased to $\sim 8 \times 10^{13}$ w/cm^2, the radiation is almost complete recombination. The temperatures, as determined from the slope of the absorption curve after subtracting out the contribution from the line radiation, are 600 eV and are essentially independent of the wavelength. Only a slight dependence of temperature on intensity is observed in the $4 - 8 \times 10^{13}$ w/cm^2 intensity range.

The intensities of the lines are of particular interest. Since the radiation temperatures are almost the same, we expect the line intensities to be proportional to $n_e n_{i,j} V$, where n_e is the electron density and $n_{i,j}$ is the

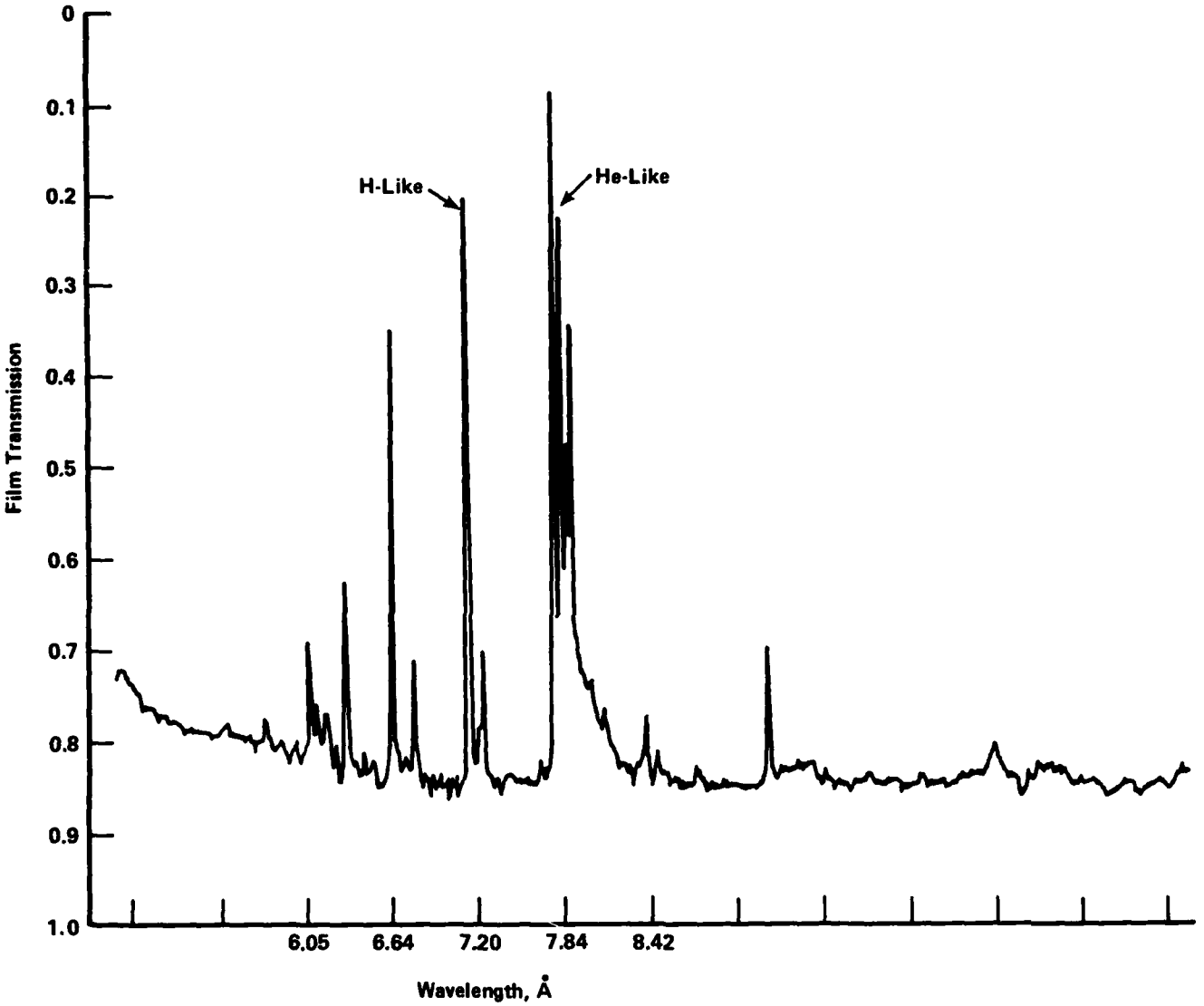

FIGURE A-1. DENSITOMETER TRACE OF Al X-RAY SPECTRUM

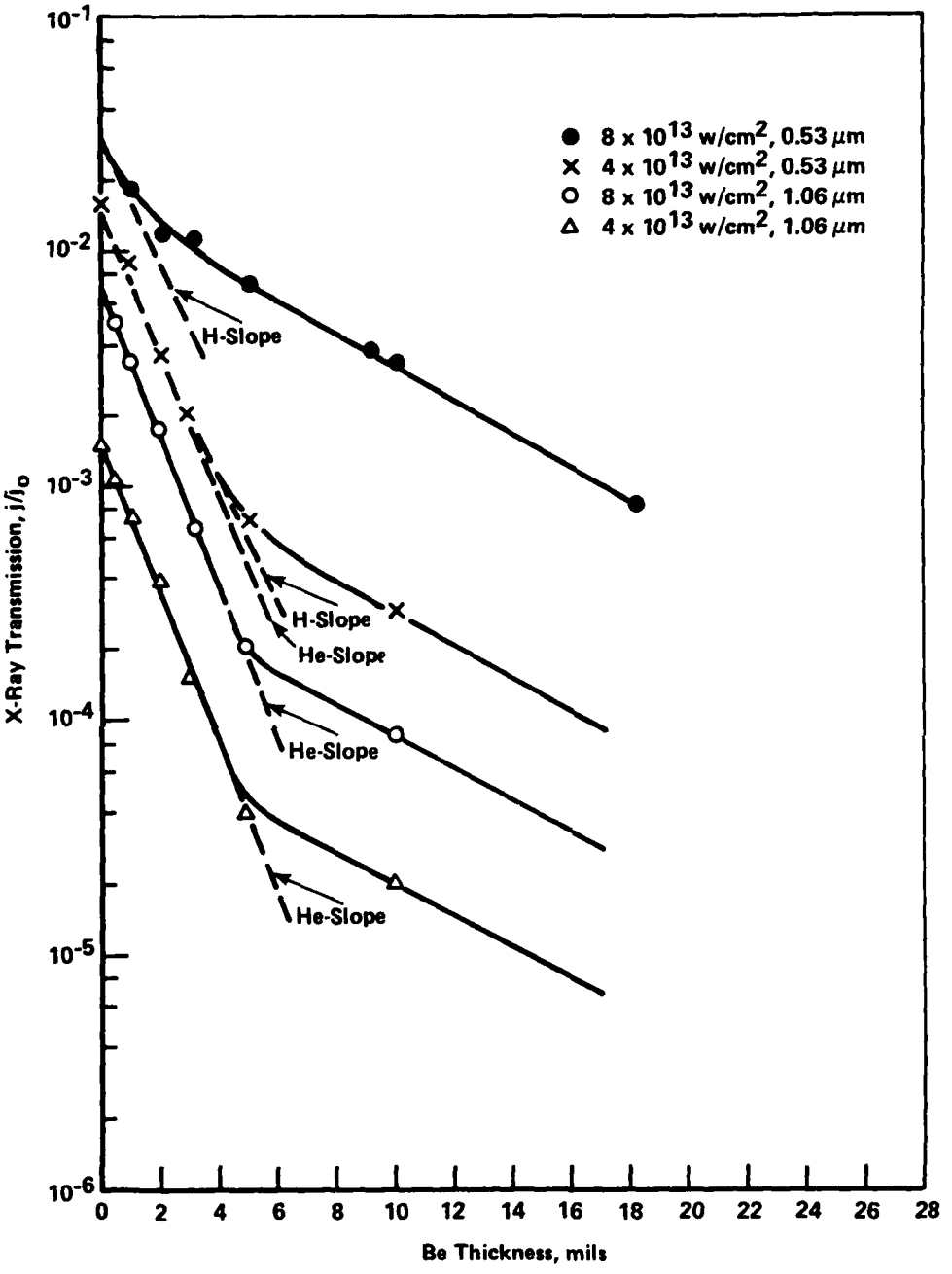

FIGURE A-2. Al X-RAY TRANSMISSION THROUGH Be FOILS

density of ions in ionization state j. At a given temperature, the effective radiation volume, V, would be expected to be strongly dependent only on focal spot size and pulse width because the relative expansion is closely related to the ion thermal velocity. For $\sim 4 \times 10^{13}$ w/cm^2 the intensity ratio of the line radiation at .53 μm to that at 1.06 μm is ~ 11 indicating that the radiation in the .53 μm use takes place from a region of about four times the density. This general result is expected since the critical density is proportional to $n\nu^2$ (assuming that the H- and He-like transitions have approximately the same probability). The sharp drop in line emission with only a small change in temperature as the laser intensity changes from 8 to 4×10^{13} indicates that the radiating zone shifts to the less dense zone in front of the critical density region near the temperature peak.

Perhaps the most interesting observation from Figure A-2 is the implied transition from a time dependent corona radiating plasma with 1.06 μm laser light incident to nearly steady state coronal plasma with 8×10^{13} w/cm^2 of 0.53 μm laser light incident. The steady-state ratio between consecutive ions in a corona model plasma may be represented by:

$$\frac{n(z,y)}{n(z+1,y)} = 7.87 \times 10^{-9}\ \chi(z,g)^2\ \left(\frac{\chi(z,g)}{kT_e}\right)^{3/4}\ \exp\ \left(\frac{\chi(z,g)}{kT_e}\right)$$

where $\chi(z,g)$ is the ionization potential of the ion of charge Z in its ground level g.

The temperature at which the population densities of the hydrogen-like state and the base nuclei are equal is shown in Figure A-3.[3] At 600 eV the corona model predicts a ratio of H-like to He-like ions of ~ 0.25 and a ratio of completely stripped to H-like ions of ~ 0.2. This indicates that the plasmas generated by the 1.06 μm laser pulse is not in coronal steady state. The 0.53 μm laser pulse at the 4×10^{13} w/cm^2 level appears close to the corona steady state. Since the relaxation time, τ, to the final state is given approximately by

$$\tau \sim 10^{12}/n_e \quad ,$$

it is not surprising that the higher density radiating regimes are closer to corona steady state. At the 8×10^{13} w/cm^2 level for 0.53 μm laser light the

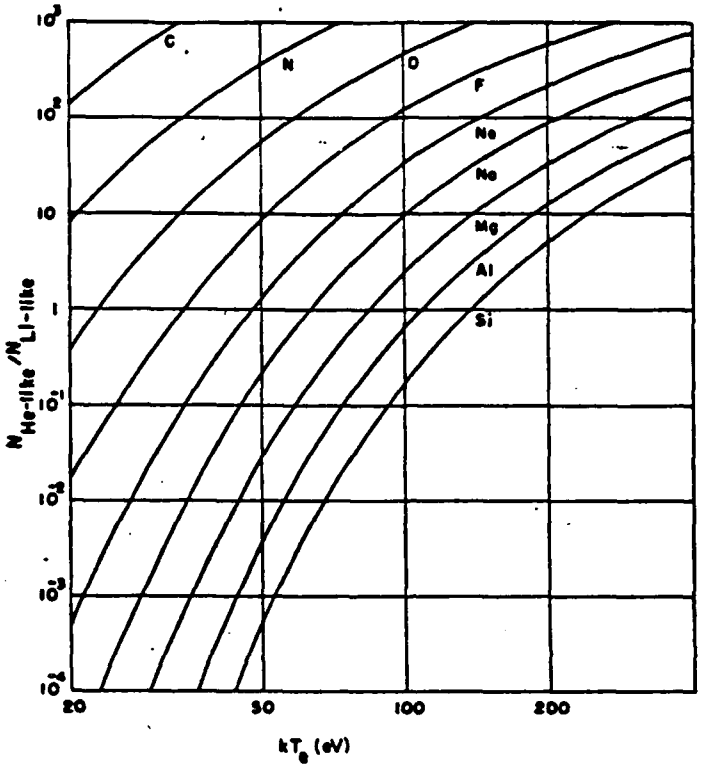

A-3a. Predictions of the Coronal Equation for the Relative populations of the Heliumlike ion to the Lithiumlike Ion as a Function of kT_e.

FIGURE A-3. CORONAL EQUATION PREDICTIONS OF RELATIVE ION POPULATIONS

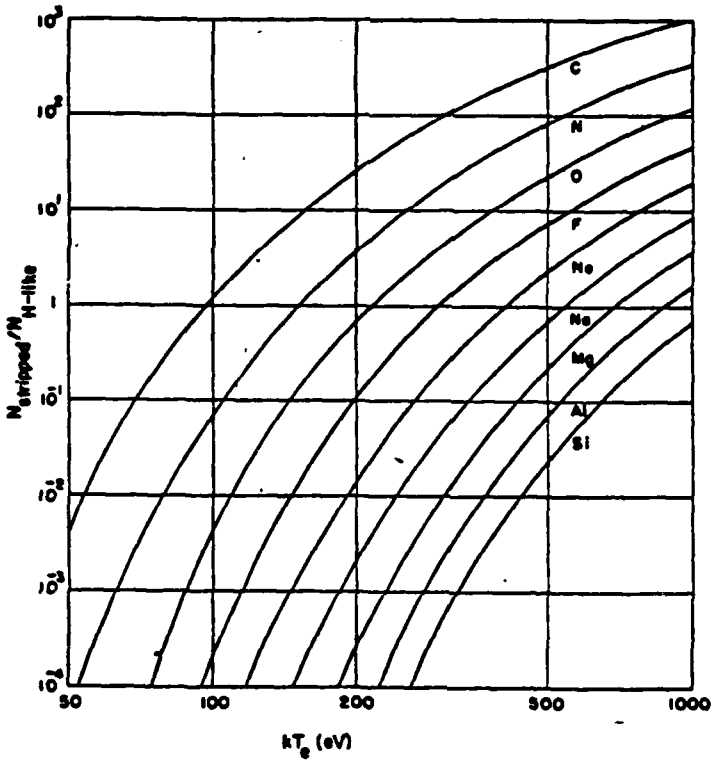

A-3b. Predictions of the Coronal Equation for the Relative Populations of the Completely Stripped Ion to the Hydrogenlike Ion as a Function of kT_e

FIGURE A-3. (Continued)

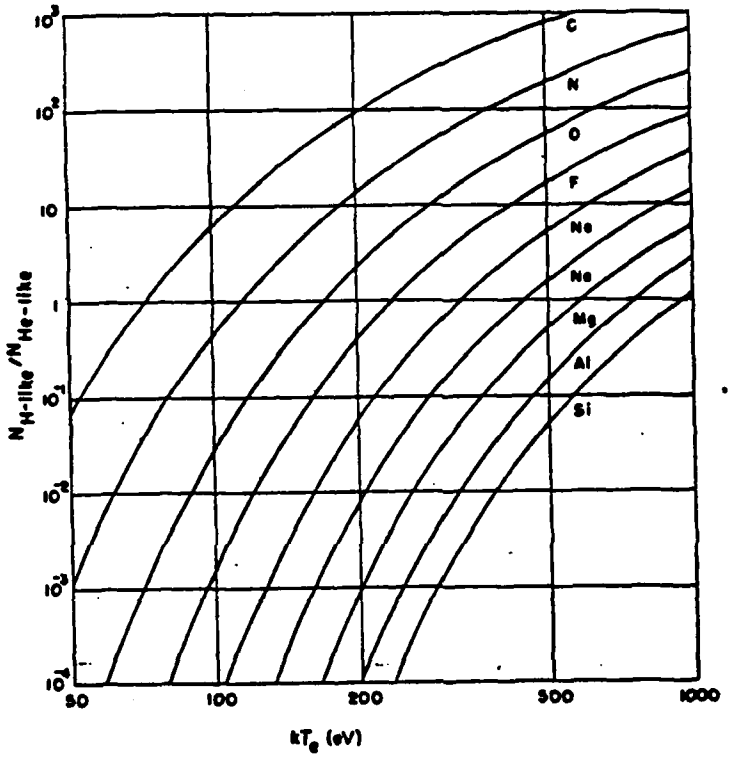

A-3c. Predictions of the Coronal Equation for the Relative Populations of the Hydrogenlike Ion to the Heliumlike Ion as a Function of kT_e

FIGURE A-3. (Continued)

radiating plasma is stripped further than should be allowed by the temperature. This appears to show that the ions are stripped in a region of the plasma where the temperature is about 1 keV, but because of the lower transition rate for recombination radiation, the bulk of the radiation is emitted as the plasma expands and the electrons cool. Spatially resolved x-ray experiments are needed to confirm the phenomenology.

The L-line experiments with Cu targets are summarized in Figures A-4, A-5, and A-6. Copper was already determined to be at the L peak of the conversion efficiency versus Z curve for x-rays above 1 keV and a power density of 10^{14} w/cm^2. It is not surprising that the radiation temperature is about 900 eV at 10^{14} w/cm^2 with 1.06 μm, because $e^{-x_{ij}/kT}$ is very nearly one for most of the L line transitions. The 900 eV temperature would cause 80 percent of the Li-like ions to be stripped to the He-like states in corona steady state. This is again a demonstration that the ions have not reached steady state. In the case of the 0.53 μm laser light, the situation is more complicated. The emitted radiation in the 10^{13} w/cm^2 incident laser light range appears to be essentially independent of incident wavelength. It is not surprising that the effective radiating temperature is about the same. Where there is an exponential dependence on temperature, the predominant radiation will tend to come from that region where the slope of the intensity variation with temperature begins to level. It is surprising that the conversion efficiency of laser light to x-rays is almost the same. This would suggest that the thermal conductivity is sufficiently high that temperature equilibration is more rapid than the ion state equipartition time, so that the exact location of the absorption does not appreciably affect the temperature or ionization state of the radiating regions. The one-dimensional "flash" calculations do <u>not</u> confirm this "quasi-isothermal" condition (Figure A-7).

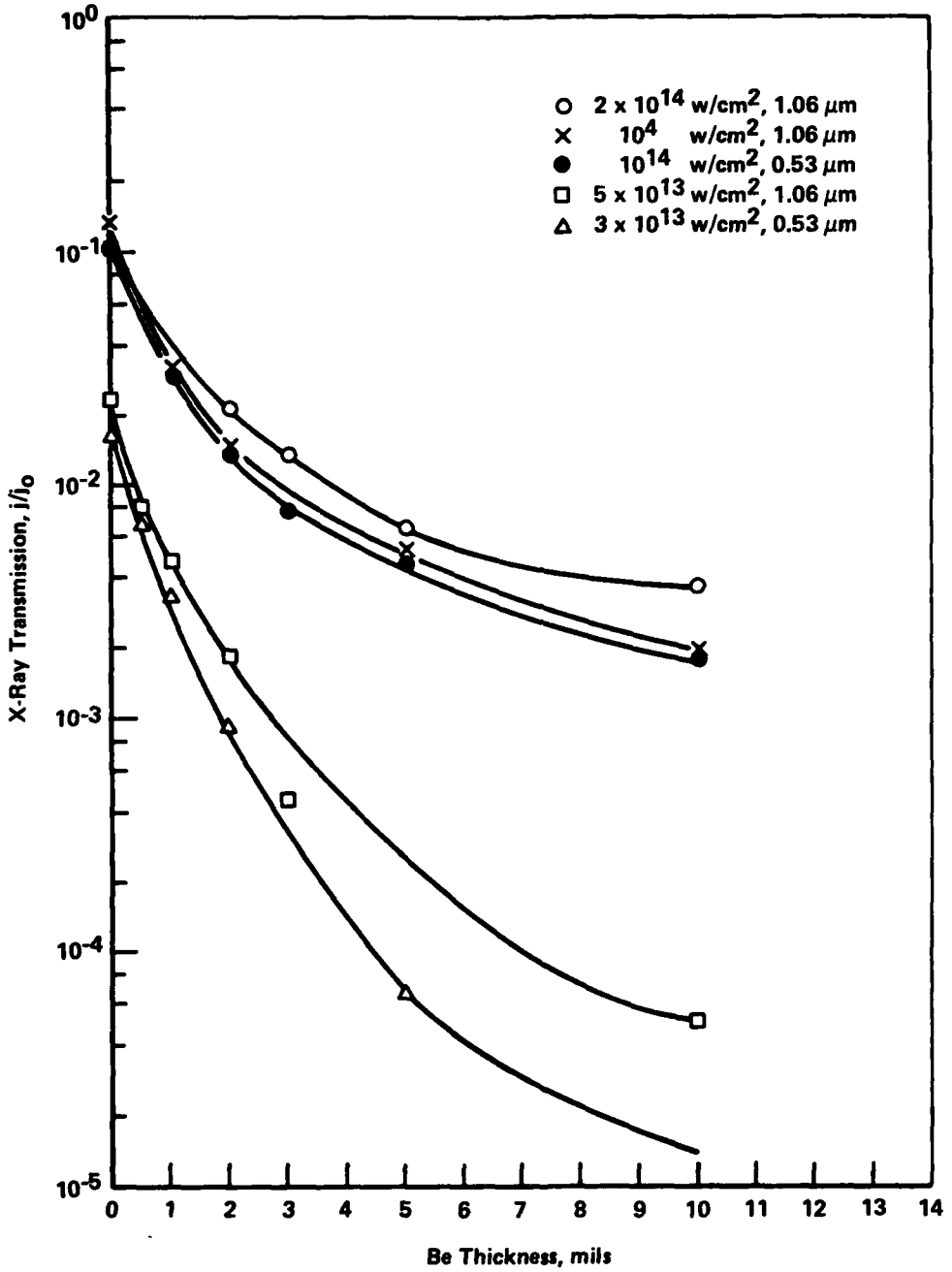

FIGURE A-4. Cu X-RAY TRANSMISSION THROUGH Be FOILS

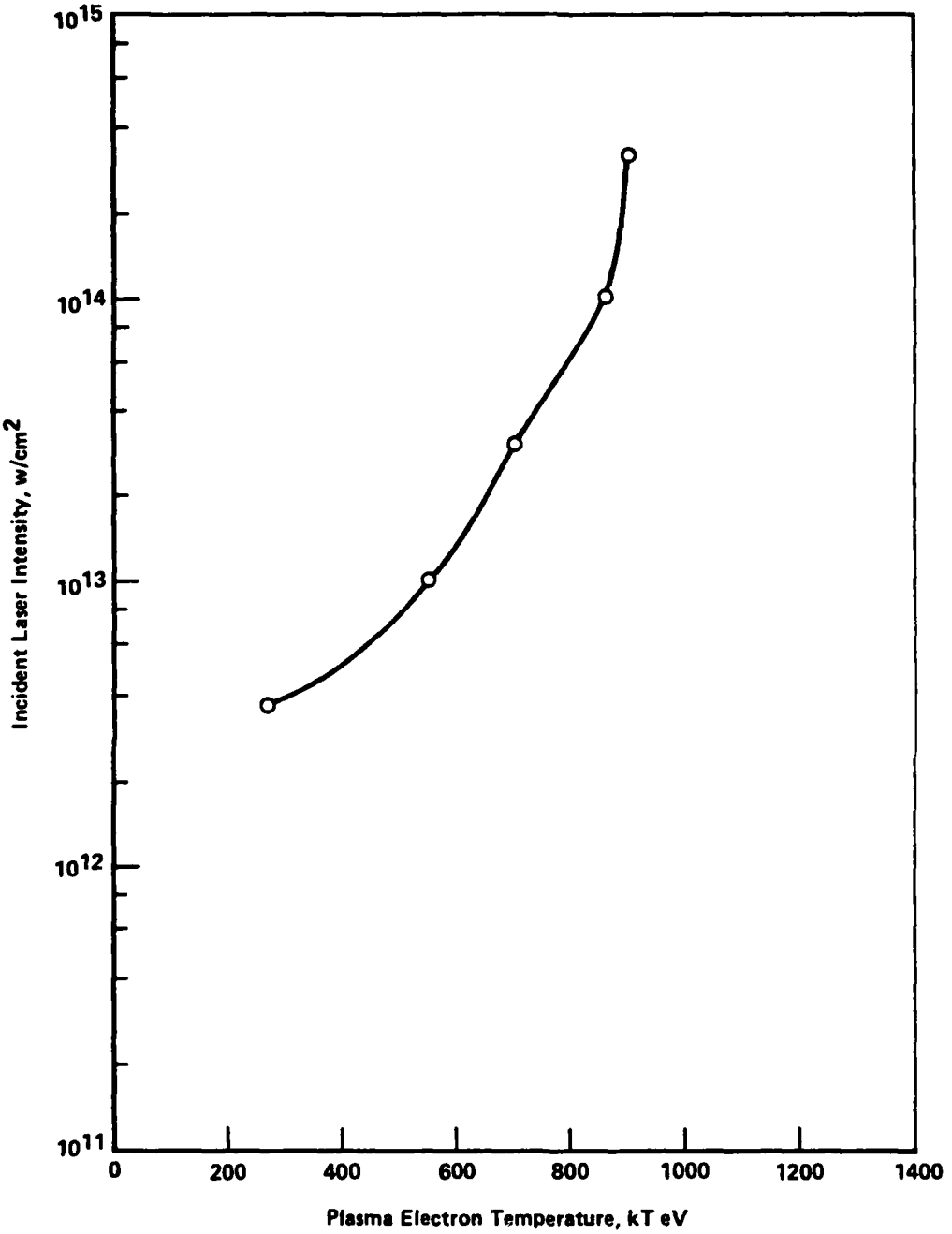

FIGURE A-5. RADIATING PLASMA TEMPERATURE VERSUS INCIDENT LASER INTENSITY FOR Cu TARGETS

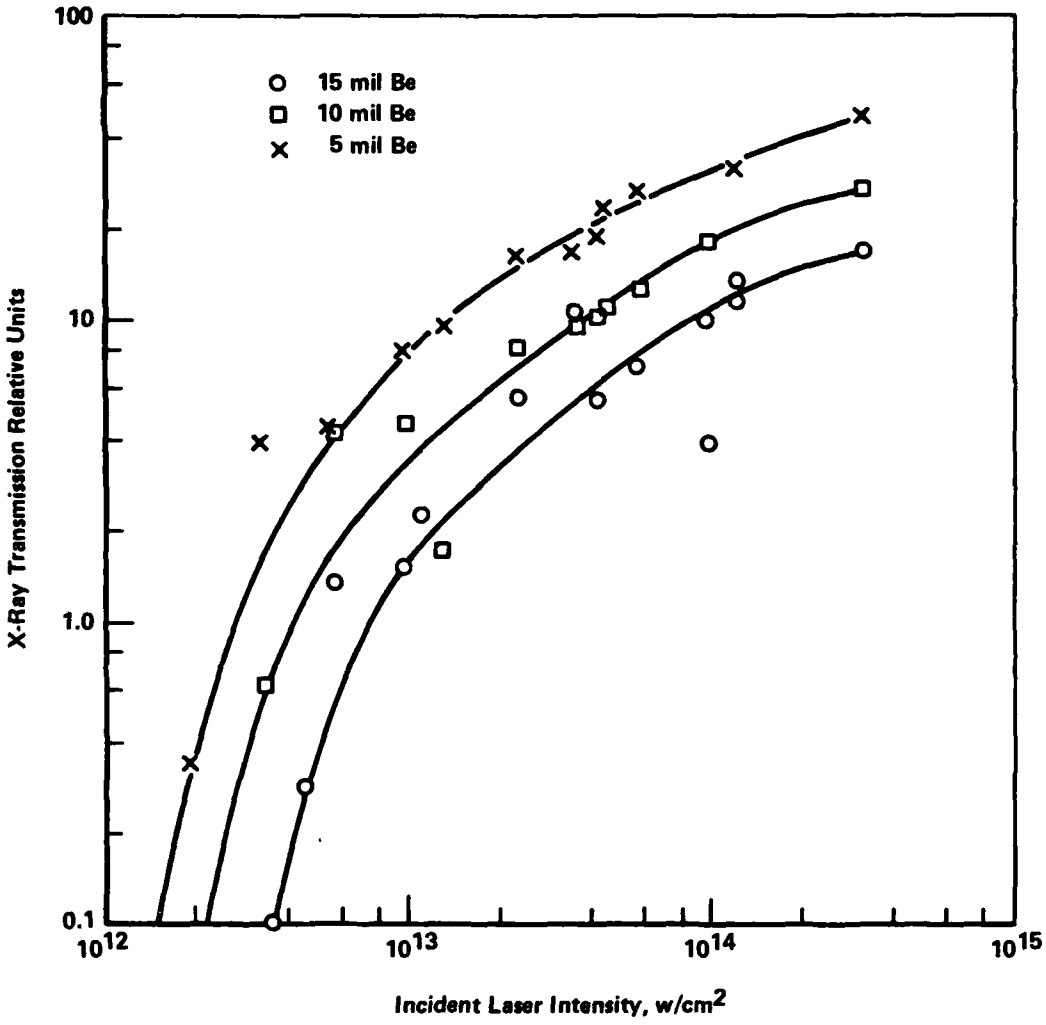

FIGURE A-6. Cu X-RAY TRANSMISSION THROUGH THICK Be FOILS FOR 1.06 μm LASER PULSES

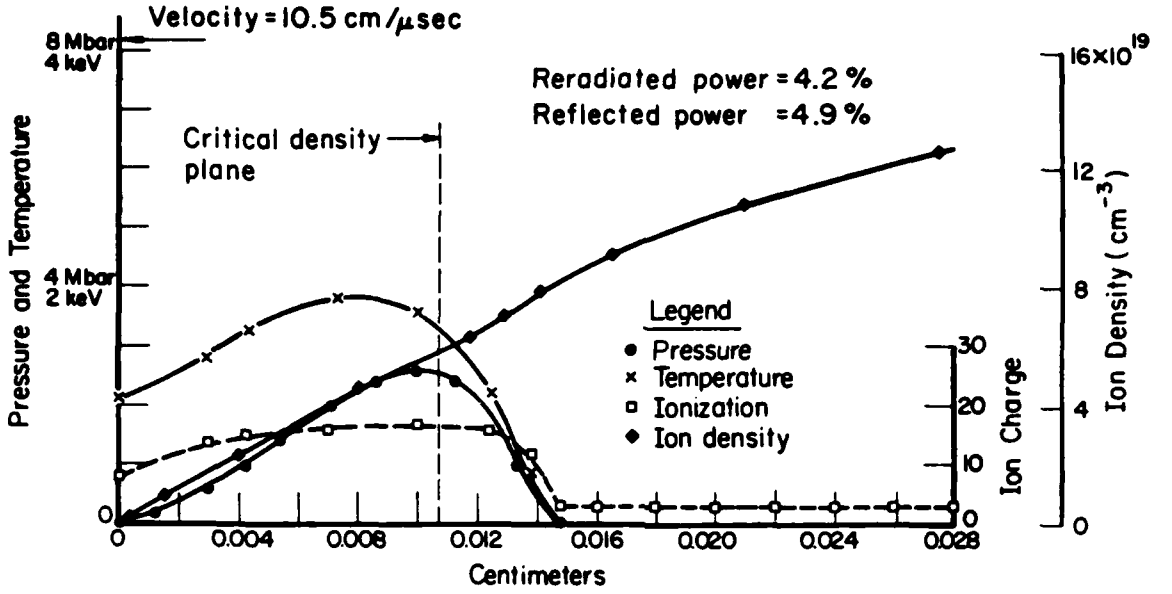

(a) Time = 33.4 Picoseconds

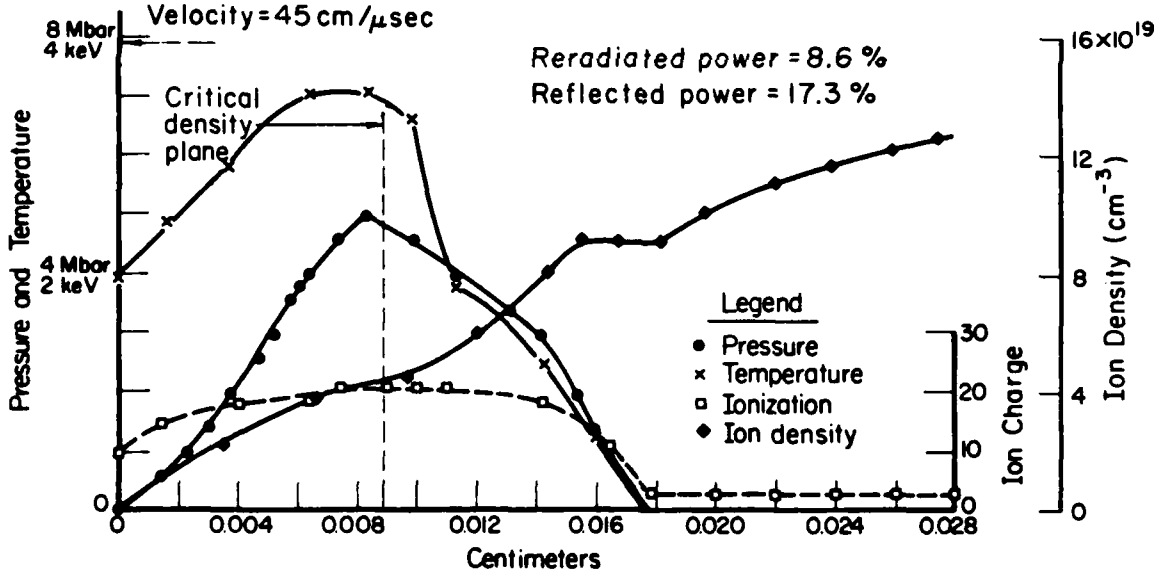

(b) Time = 86.8 Picoseconds

FIGURE A-7. NONEQUILIBRIUM IRON CALCULATION: TIME-DEPENDENT IONIZATION

Incident laser flux = 1.05 x 10^{14} watts/cm^2
Wavelength = 1.06 microns

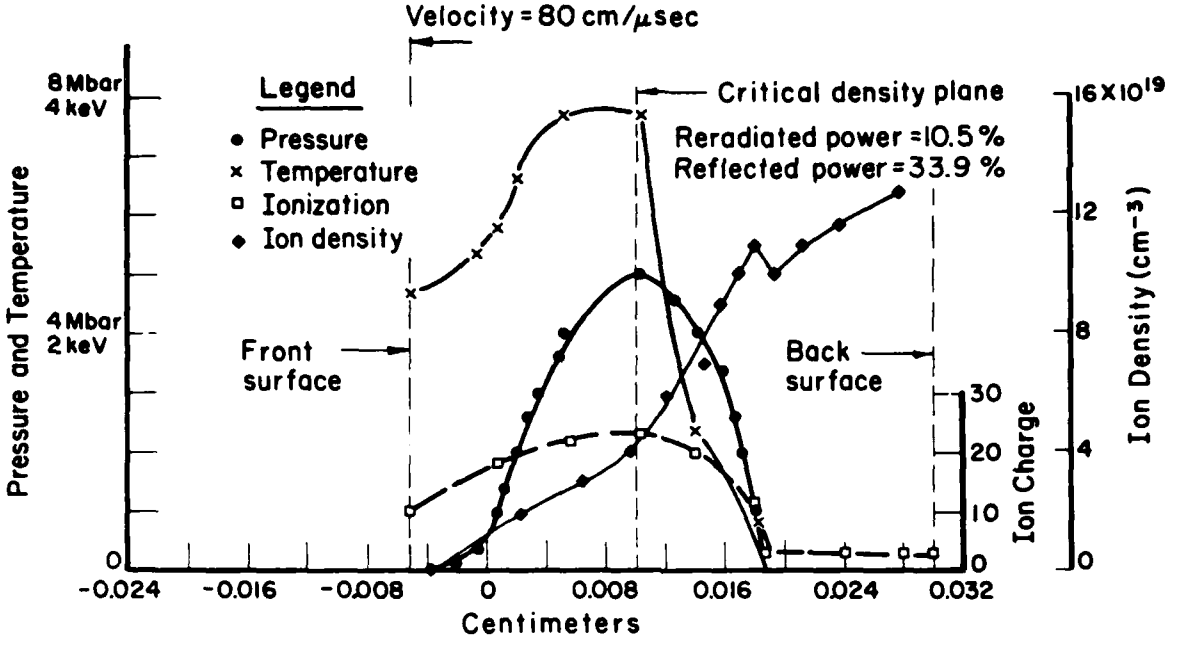

(c) Time = 135 Picoseconds

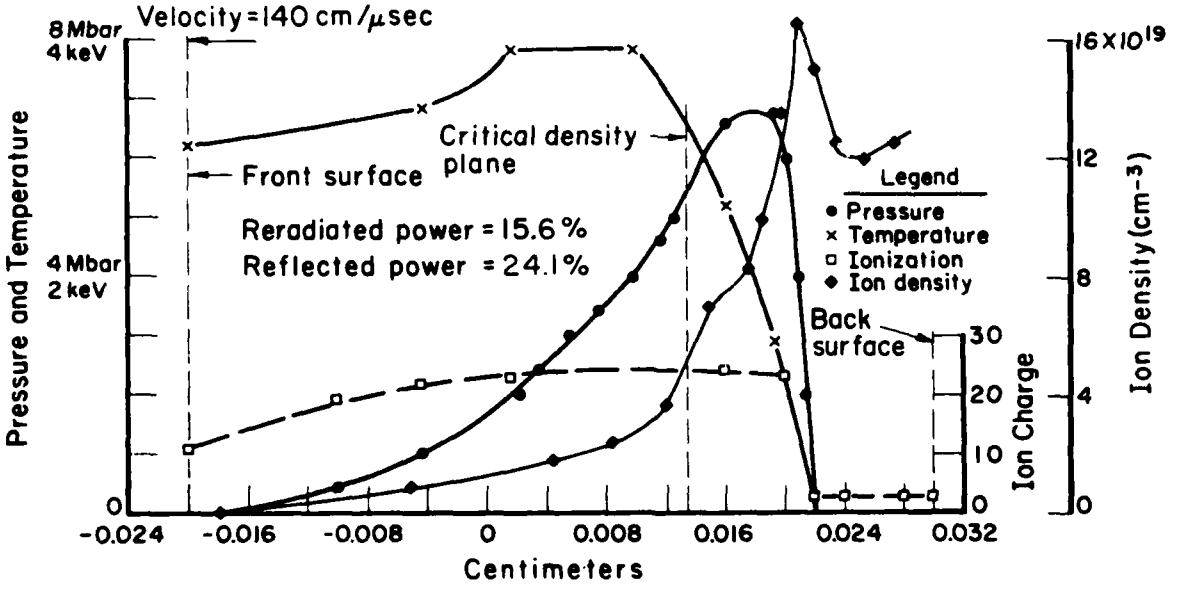

(d) Time = 265 Picoseconds

FIGURE A-7. (Continued)

REFERENCES

(1) Boiko, V. A., Pikuz, S. A., and Safronova, U. I., "The Analysis of Satellites to the H-Like Ion Resonance Lines Observed in the X-Ray Region, Mon. Not. R. Astr. Soc., 118, 107-120 (1978).

(2) Bhalla, C. P., Gabriel, A. H., and Presnyakov, L. P., Mon. Not. R. Astr. Soc., 172, 359 (1975).

(3) Stratton, T. F., Plasma Diagnostic Techniques, R. H. Huddlestine and S. L. Leonard, Eds., Chapter 8, Academic Press, New York (1965).

APPENDIX B

LASER-PLASMA X-RAY SOURCE FOR X-RAY LITHOGRAPHY

Laser-plasma x-ray source for x-ray lithography

Harold M. Epstein

Electronics Department, Battelle's Columbus Laboratories
505 King Avenue, Columbus, Ohio 43201

Abstract

Laser-plasma x-ray sources have been evaluated for submicron x-ray lithography. Exposure machines based on available, repetitively pulsed lasers of reasonable cost appear to be attractive. These machines would make full wafer exposure levels in times consistent with present manufacturing requirements.

Introduction

X-ray lithography is a logical extension of the near contact optical and U.V. printing techniques into the soft (0.25 - 3.0 keV) x-ray regime.[1,2] The technology has advanced to the point where submicrometer line width patterns can be produced with a throughput of more than one 75 mm diameter wafer level per minute. An x-ray exposure machine with these capabilities, using a Pd-Lα anode in a 4.5 kW electron beam x-ray unit, was developed at Bell Laboratories.[3,4]

Although electron beam x-ray sources may be satisfactory for the first generation of machines, future developments will almost certainly depend on the higher brightness, non-conventional x-ray sources such as pulsed plasmas.[5-10] Conventional production of line width patterns significantly smaller than 1 micrometer requires combinations of softer x-rays, smaller source diameter, and higher time average x-ray power and brightness that are difficult to achieve with electron beam x-ray source.

This paper discusses the optimization of high pulse rate laser-plasma x-ray sources for submicrometer x-ray lithography. Because it is not possible to optimize the x-ray source isolated from the other components of the x-ray lithography exposure machine, such topics as windows, masks, and photoresist will also be discussed. In many situations, the applicable materials research is not available to adequately match the source to a systems component such as the photoresist or mask. When these situations occur, the optimization will be based on the present component status, but an evaluation of the benefits from expected improvements will be included.

The general advantage of the high pulse rate laser-plasma x-ray source over conventional electron beam x-rays are: (1) the small source diameter drastically reduces the penumbra effect and allows short source-mask distances for step and repeat exposures[2]; (2) the small source diameter allows the x-rays to be extracted from the vacuum through a set of differentially pumped orifices eliminating the need for windows; (3) the x-ray absorption cross-sections of most photoresist components are much higher for the soft x-rays providing greater energy absorption; (4) the photon statistics per unit of absorbed energy in the photoresist is better; and (5) for a given absorber thickness on the mask, the contrast ratio between transmitted and absorbed areas in the pattern is greater for soft x-rays. In addition to these tangible advantages, several other factors favor the laser-plasma x-ray system. Laser technology is relatively new and growing at a rapid rate, so that order of magnitude improvements in average power can be expected in the near future, whereas the electron beam x-ray machine is a rather stable technology. Also, a laser system can be installed outside of a clean room with the beam brought in through an enclosed pipe, saving expensive clean-room space.

Laser-plasma phenomonology

During the optimization process, it is necessary to relate trade-offs between spectral characteristics, efficiency, and laser characteristics. Thus, the physical mechanism that converts the laser light into x-rays is of interest. Briefly, a specially tailored leading edge of the focused laser pulse vaporizes and ionizes the surface of the target creating a low temperature plasma. The plasma that is created absorbs a large fraction of the remainder of the laser pulse and is heated to a temperature slightly below 1 keV (1.2×10^7 K) at a typical laser radiation intensity of 10^{14} w/cm^2, as seen in Figure 1. X-rays are produced in this high temperature plasma by bremsstrahlung, recombination radiation, and line radiation, all of which originate from electron-ion collisions.[11]

Unless specified otherwise, the reference system consists of 1.06 μm neodymium laser light incident on a copper target at an intensity of 10^{14} watts/cm^2. The x-ray spectrum

generated with a copper target has a large number of intense spectral lines in a spectral band centered at approximately 1.2 keV (Figure 2).. The spectral lines are L-lines emitted from highly ionized species of copper. The band of lines can be moved up or down in energy with targets of higher or lower atomic number. However, Figure 3, which plots conversion efficiency versus atomic number Z, shows copper (Z = 29) to be the optimum element for converting neodymium laser light into x-rays above $h\nu \simeq 1$ keV, assuming an incident intensity of 10^{14} watts/cm^2.

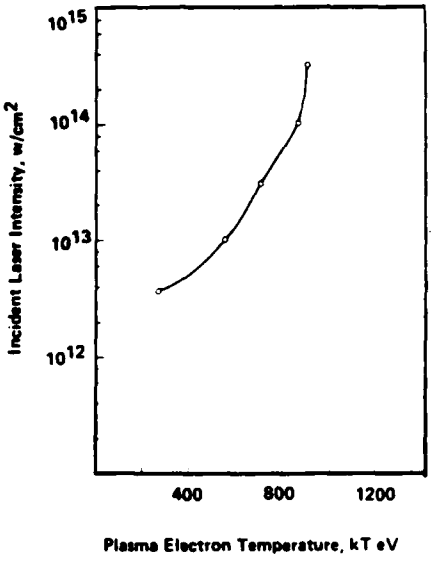

Figure 1. Radiating plasma temperature versus incident laser intensity for Cu targets

The spectral lines are emitted from a plasma layer of electron temperature Te $\sim$ 1 keV and electron density $n_e \sim 10^{21}$ cm^3 located near the leading edge of a thermal diffusion front that advances through the low temperature plasma during the lifetime of the laser pulse. To understand the reason for the peaks in Figure 3, it is helpful to realize that the L-lines are mostly caused by inelastic collisions between free electrons and ground state ions. The collisions excite bound electrons from the L-shell to the M-shell, and the x-rays are produced by the spontaneous radiative decay of M-shell electrons back to the L-shell. Targets with Z above the copper peak have energy gaps between the L and M subshells that are too wide to be efficiently excited. Targets with Z below the peak have the problem that the various energy gaps between L and M subshells increasingly fall below 1 keV as Z decreases. These very soft x-rays are unable to penetrate any practical mask substrate and for present purpose need not be considered. Also, the depletion of L-shell populations below the peak causes a decrease in conversion efficiency. The peak in K-shell conversion efficiency at a Z of about 13 can be explained in terms of the K and L subshells in a similar manner. The K-shell peak is much lower in conversion efficiency, but the x-ray emissions are more energetic. An Al target emits predominantly He-like Al Kα line radiation at 1.6 keV. The K-peak efficiency can be increased substantially by using shorter wavelength laser light which penetrates to a denser portion of the plasma. However, most of the radiation is continuous recombination radiation with a low energy cutoff at 1.6 keV.

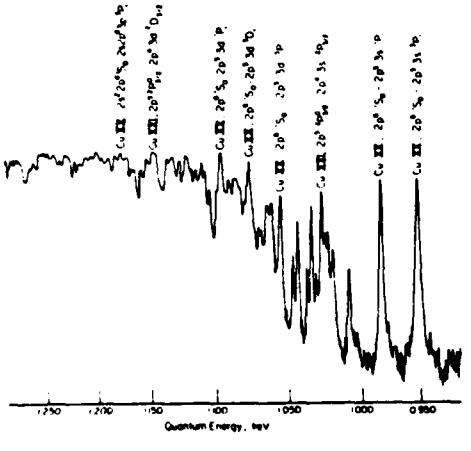

Figure 2. Densitometer tracing of bent crystal spectrograph of x-ray produced from copper target with neodymium laser pulse

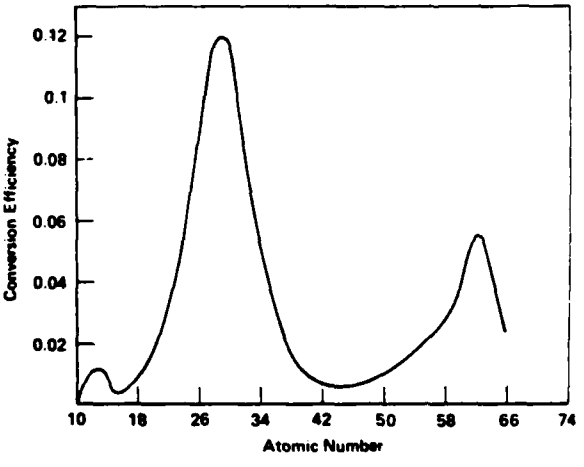

Figure 3. Dependence of x-ray conversion efficiency above 1 keV on atomic number for 1.06 μm, 10^{14} w/cm^2

X-ray interactions

In the x-ray energy range of importance to microlithography, the dominant x-ray interaction mechanism is photoelectron emission. Scattering is negligible, so that x-rays travel in essentially straight lines until captured. Fluorescent yields are also very small for low energy x-rays (less than a few percent) so for all practical purposes, the x-ray energy is converted into electron energy at the first interaction. Normally, the excited atom

returns to the ground state by emission of Auger electrons. The photoelectron and the Auger electrons expose the photoresist. The range of these electrons and diffraction of x-rays at the mask determine the limit of resolution for an ideal x-ray source.[12]

The cross section for capture of the x-ray by electrons varies with the photon wavelength and exhibits large jumps at critical wavelengths or edges. Between the edges, the cross section increases roughly as the cube of wavelength.

In the evaluation of the various components of an x-ray lithography exposure machine, it is necessary to evaluate the attenuation of the x-ray beam through a component. For a monoenergetic x-ray beam, the attenuation I/I_o is given by

$$I/I_o = e^{-\alpha(E)x}$$

where I_o is the incident flux in J/cm^2, α is the absorption cross section at energy E and x is the attenuation thickness. A more complex spectrum can be divided into energy bands and treated numerically. However, the general exponential shape of the laser-plasma x-ray envelope permits a shortcut for optimization calculations. The three radiation processes have the same statistical exponential spectral dependence for an optically thin plasma of thermal energy (kT) in keV. For a collimated source,

$$I/I_o = \int_0^\infty \exp\left[(-\alpha x - h\nu/(kT)\right] d(h\nu)$$

where $(h\nu)$ is the photon energy (keV). For a material with no edges near 1 keV, $\alpha \approx C_1 (h\nu)^{-3}$, where C_1 is the absorption cross section for the material at 1 keV.

The x-rays emitted from the plasma fall off exponentially with increasing energy, while the x-ray transmissivity of the absorber, $T(h\nu)$ is controlled by the photoelectric absorption cross section and falls off rapidly with decreasing energy. The transmitted x-rays fall in a narrow band as shown in Figure 4. The peak energy of this transmission band, $(h\nu)_m$, is given by

$$(h\nu)_m = 1.32\ C_1^{1/4}\ x^{1/4}\ (kT)^{1/4} \qquad (1)$$

Because of the sharply peaked integral, when kT is less than $(h\nu)_m$, the integral can be evaluated by expanding in a Taylor series about $(h\nu)_m$ (saddle point method), giving

$$I/I_o \simeq 1.5\ (kT)^{5/8}\ x^{1/8}\ C_1^{1/8} \exp\left[-1.75\ C_1^{1/4}\ x^{1/4}\ (dT)^{-3/4}\right] \qquad (2)$$

Now, if we consider a photoresist without absorption edges in the region of $(h\nu)_m$, the absorbed dose, $D(J/cm^3)$ at the surface is given by

$$D \simeq .69\ (kT)^{-1/8}\ x^{-5/8}\ C_1^{-5/8}\ C_2\ I_o \exp\left[-1.75\ C_1^{1/4}\ x^{1/4}\ (dT)^{-3/4}\right] \qquad (3)$$

where C_2 is the absorption coefficient of the resist at 1 keV. If the exponent is less than ~ 1, the approximation fails.

Resolution

Lack of sharpness in the image of the mask pattern can result from several sources. The primary geometrical effects are the following:

(1) Source size - the replication error, δ, due to penumbra effects of source size is $\delta = DL/R$. The symbols are defined in Figure 5. This error is decreased when a high λ photoresist is used. The source size becomes a particular problem for step and repeat exposures where R is small. Laser x-ray sources which are about 1/100 the size of conventional sources essentially eliminate this error.

(2) Wafer warpage - warpage causes a shift and distortion of the pattern projected on the wafer. The warpage replication error δ_w is $\delta_w = w \tan\theta$ where w is the displacement due to warpage (Figure 6). Warpage can be minimized by vacuum back plates to hold the wafer and by use of step and repeat exposures which effectively reduce all dimensions.

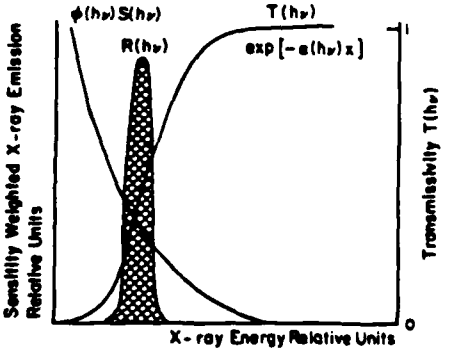

Figure 4. Sensitivity weighted x-rays on photoresist

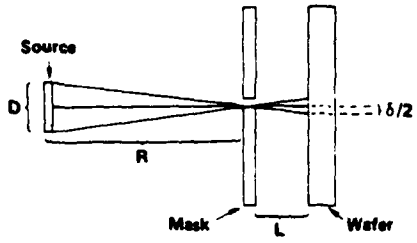

Figure 5. Replication error due to source size

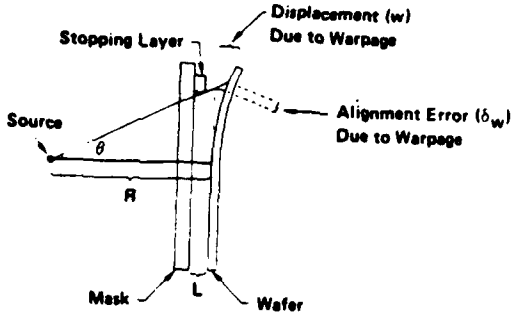

Figure 6. Alignment error due to warpage

(3) Finite opaque layer penumbra - the thin absorbing layer that forms the pattern on the mask causes an "unsharpness" in the image projected on the wafer (Figure 7). The replication error due to this effect depends on the absorption coefficient of the stopping layer and on the gamma of the photoresist. Assuming that a contrast factor of ten is needed for a good image, this pattern thickness unsharpness δ_p is given by

$$\delta_p = \frac{2.3 \tan \theta}{a_p} .$$

The absorption cross section of the pattern layer is very high for the soft x-rays emitted by laser-plasma sources. Thus, δ_p is minimized.

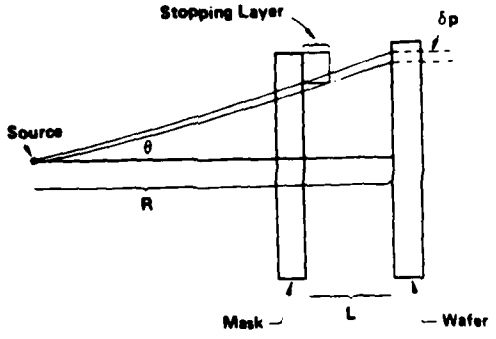

Figure 7. Replication error due to finite thickness of stopping layer

(4) Fresnel diffraction - there is a replication error, δ_F, due to Fresnel diffraction. Since R >> L, this error is proportional to $\sqrt{\lambda L}$ with a proportionality constant on the order of 1. A diffraction error of 0.1 to 0.2 micrometers can be expected for the mask wafer spacings currently considered.

(5) Mask alignment - a replication error due to mask alignment is independent of the x-ray source, provided that the source does not impose physical constraints on the alignment system.

In addition, there are several potential sources of unsharpness which are not related to geometry.

(1) Range of emitted electrons - this effect is very small for soft x-rays[12] of the order of 5 to 65 nm.

(2) Finite size of photoresist molecules - the effective resolution cannot be better than the diameter of the resist molecules.

(3) Photon statistics - if the exposure is to avoid a statistical mottle, it is necessary to have many photons absorbed in each resolution element. Statistically, 1/e of the elements will have an exposure variance greater than $\sqrt{N}/N$, where N is the average number of absorptions in each element. In most photoresists, the exposure sensitivity is so low that photon statistics is not a limiting factor.

Basic lithographic exposure system

The basic configuration used in generating x-rays for lithography is shown in Figure 8. In our reference system, 1.06 micrometer wavelength laser pulses with an energy of 0.3 joules and a pulse width of 0.2 nanoseconds are focused onto a copper target to a spot size of about 40 μm. Approximately 25 percent of the incident light is converted into x-rays in the 0.3 to several keV range. Approximately 10 of the 25 percent lies between 1 and 2 keV.

The target is a relatively large cylinder that advances on a helical drive to present a fresh, nearly flat surface area to successive laser pulses. Since each laser pulse destroys only about 10^{-4} cm^2 of target area, a cylinder with 100 cm^2 of surface area will give about a million x-ray pulses.

A mask/wafer assembly (Figure 8b) is placed 5 cm from the source. This distance maintains δ_b less than 0.1 micrometer and allows a reasonable number of step and repeat exposures for the wafer. The x-ray outputs which we cited refer to x-rays emitted into the 2π steradians facing the mask/wafer assembly.

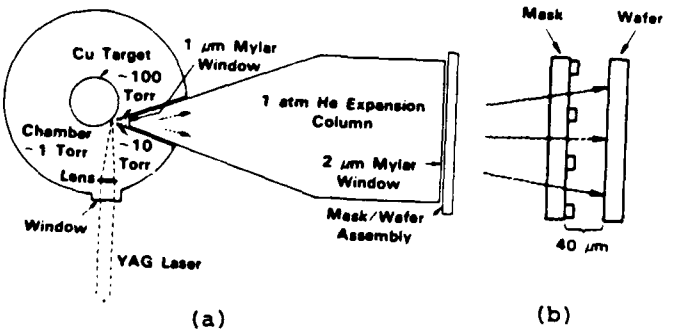

Figure 8. Experimental configuration with differentially pumped orifices

The small source diameter permits a solution to the troublesome problem of designing an x-ray window to bring the soft x-rays out of the vacuum and into an atmospheric pressure helium expansion chamber. Figure 8 shows the x-rays directed out of the vacuum chamber through a set of differentially pumped orifices. The first hole has a diameter of $\sim$ 1 mm and is located less than 2 mm from the source, so that all of the x-rays directed at the desired portion of the mask will pass through the holes.

Laser parameters

For the high-average power required in x-ray lithography, it is advantageous to use a low pulse energy, high repetition rate laser. It can be seen from Figures 3 and 9 that the preferred target intensity is $\sim 10^{14}$ watts/cm^2 for 1.06 μm laser light. Conversion efficiencies and temperatures fall off rapidly as intensities fall below this level, while intensities much greater than 10^{14} lead to extra costs and to complications worth avoiding. The conversion efficiency depends on several other parameters besides peak intensity. Since the critical density boundary is moving during the pulse, it is desirable to have the focusing cone angle as small as possible to maintain the focal intensity. On the other hand, a high f number system yields a large focal spot for a given beam divergence Δ, and diameter D_b. The optimum f number of the lens, f_{opt}, is given by

$$f_{opt} \simeq \left(\frac{v\tau}{D_b \Delta}\right)^{1/2} \tag{3}$$

where v is the velocity of the critical intensity boundary and τ is the laser pulse width (FWHM). For a Cu target under conditions of interest, $v \sim 3 \times 10^7$ cm/sec.[11] To exceed the 10^{14} w/cm^2 peak focused intensity with an optimum lens and a Cu target, the laser energy, E_L, should meet the following conditions:

$$E_L > 10^{14}\ \tau^2\ D_b\ v\ \Delta \tag{4}$$

Wave length is not considered in this scaling relationship, but for a Cu target, no significant difference in conversion efficiency or temperature was observed when the irradiation wavelength was changed from 1.06 to 0.53 μm. For elements whose primary x-ray emissions are from the K-shell, efficiencies are appreciably improved at shorter wavelengths.

Some care must be exercised in using this scaling relationship for pulse widths appreciably below 10^{-9} seconds. The difficulty is that the plasma radiates most of the x-rays at an electron density near $n_e \sim 10^{21}$ cm^{-3}, so that the characteristic time required for the radiating ions to strip down to a quasi-steady degree of ionization is approximately $10^{12}/n_e \sim 10^{-9}$ seconds.[13] However, only a thin layer of matter in the plasma is radiating x-rays significantly at any given time during the pulse, and the time that is spent in the critical zone is a small fraction of a nanosecond. The phenomenological description of the layers that successively radiate the x-rays is the same for pulse widths down to about 0.1 nanosecond.

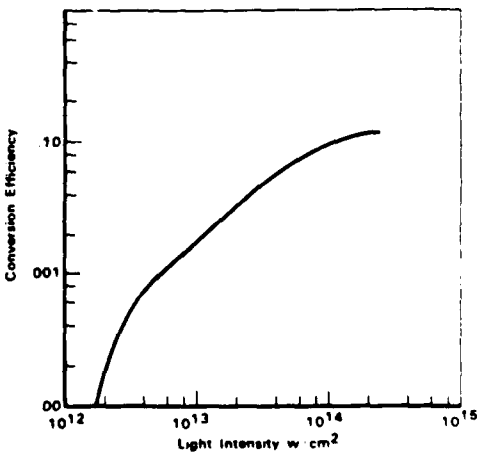

Figure 9. Conversion efficiency to x-rays above 1 keV for 1.06 μm laser light

We are now in a position to discuss the selection of a candidate laser. The highest average power laser available as a commercial laser which meets the criteria of Equation 4 is the Quantel 402 DP with a pulse rate of 10 Hz, a pulse width of 0.2 nanoseconds and a pulse energy of .3 Joule. At the 10 percent conversion efficiency, this would yield 0.3 watts of x-ray power. The cost of this system is approximately $100,000. Several systems under development promise to provide higher average powers within a few years and still meet the criterion of Equation 4. The multiple reflection slab laser system under development[14] promises average powers up to 1 Kw. Also, development of reinforced glass rods to permit an order of magnitude increase in average pumping rates could lead to a relatively inexpensive glass rods system with an average power in the tens of watts in the near future.[15] Longer range possibilities include gas lasers such as the Eximers and Iodine.

Mask/Substrate

A major limitation in submicron lithography is the thickness of the absorber mask required to produce an adequate contrast. Most masks are fabricated with electron beam lithography. Since scattering of electrons makes the production of deep vertical walls difficult, the aspect ratio achievable in the mask is one limitation to x-ray lithography. It is instructive to compare the thickness of Au and U-238 required to produce a factor of ten dose contrast in the photoresist with laser-plasma x-rays (kT - .85 keV) and Pd-Lα x-rays (2.84 keV). For the laser plasma system, the resist will be considered to be undoped and composed of low atomic number elements. The dose contrast is independent of the resist and substrate for the nearly monoenergetic Pd-Lα system, and a gold layer of 0.49 μm is needed.

The thickness of Au required on the 4 mm Si substrate for a laser plasma source is less than half that for the Pd-Lα. The difference is even larger for U-238. We have used 4 μm and 3 μm thick Si substrates for laser plasma lithography. Reference 16 discusses 2.5 μm SiC mask substrates. The advantages of thin substrates for high contrast are evident from Table 1. The largest part of the attenuation through the uncoated substrate comes from the removal of the very soft component of x-rays (less than 1 keV) which were not included in the 10 percent conversion efficiency.

Table 1. Mask contrasts and attenuations and PMMA energy deposition (plasma temperature .85 keV)

x_{Si} nm	Equivalent x_{SiC} μm	For contrast of 10 x_{Au}	For contrast of 10 x_{U-238}	Substrate Attenuation	D/I_o PMMA cm^{-1}
2	1.30	.12	.10	.21	320
4	2.61	.19	.16	.16	150
6	1.95	.27	.23	.13	88
8	5.21	.34	.28	.12	66

Photoresist

Most of the photoresists used in lithography are polymers. Resists are classified as positive or negative depending on whether their solubilities in the developer are enhanced or diminished by irradiation. When a long chain polymer is subjected to ionizing irradiation, valence bonds are broken causing the solubility of the resist in the developer to change. Since most of the bond breakage is caused by secondary electrons in either electron or x-ray exposures, the sensitivity of the resist in terms of volumetric energy absorption is not dependent on the type of radiation to a first approximation. With x-rays, the absorptions occur preferentially in the higher atomic number atoms, but the photoelectric event is in a deep subshell and the range of the Auger electrons is much greater than atomic distances.

As can be seen from Equation 3, the volumetric energy deposition rate in the resist is proportional to C_2, the x-ray cross section at 1 keV (assuming no absorption edges within the sensitivity peak, and a thin mask substrate). Doping a resist with heavy elements to increase the absorption cross section is an effective method for increasing the efficiency of resists to soft x-ray. Substituting a Th atom for one C or H atom in each methyl methacrylate unit in PMMA increases the absorption by a factor of 4.

The size of the polymer molecule in a resist plays a similar role to the size of a grain in photographic emulsions. If the number of chain scissions required to expose a molecule were independent of the molecule size, the exposure sensitivity would be proportional to

the molecule's volume or the solubility would be approximately proportional to the molecular weight.

Finally, the sensitivity can be altered by changing the chemical structure of the polymer. A Soviet study of the effect of chemical structure and distribution of carboxyl groups in resist materials exposed to laser-plasma x-rays showed very promising results.[17] The sensitivities of copolymer methylmethacrylate and methacrylic acid resists were improved to the extent that they were fully exposed by two laser-plasma x-ray pulses at a distance of 10 cm. The x-ray yield per pulse was 400 mj between 1.5 and 15 Å and the film was covered by 3 μm of Lavsan coated with 0.3 μm Al. Under these conditions, the resist exposure was under 1 mj/cm^2. This is comparable to the sensitivity of the chlorinated photoresist developed by Bell Laboratories for Pd-Lα x-ray exposures.[18]

The gamma curve for resists is usually defined as

$$\gamma = [\log D^{1.0}/D^{i}]^{-1}$$

where D^i is the initiation dose and $D^{1.0}$ is the dose for 100 percent film removal based on extrapolation of the slope at $D^{0.5}$ (see Figure 10). The γ for a resist is analogous to γ for photographic film and indicates contrast. High γ's give sharp lines.

System configuration and exposure time

We are now ready to fully specify a system, which can be constructed with essentially current technology as shown in Table 2. While higher average power lasers should soon be developed, a reasonable exposure machine can be based on the commercially available laser listed. The copper target is the best L-shell emitter. While the optimum K-shell emitter gives harder x-rays and lower mask substrate attenuation, the poor conversion efficiency and lower resist absorption make this a poor choice. If resists were to be developed with absorption edges slightly above 1.6 keV, Al might be a good target choice. However, the mask contrast would be poorer. Si is almost optimum as a mask substrate because the laser plasma x-rays fall into the notch below the Si K-edge. However, SiC is not much more absorbing and is transparent to light for interferometry alignment. The target/mask distance of 5 cm is enough to keep the source penumbra "unsharpness" below 0.1 μm, and the step and repeat area of 4 cm^2 maintains an exposure uniformity better than 5 percent. The 40 μm mask/wafer distance is chosen to correspond to industry practice.[3] The choice of photoresist is not clear because of the lack of published data in the x-ray energy range of interest. However, statistics alone would require an energy deposition of ∿ 10 J/cm^3 for 0.1 μm resolution. If the exposure through the resist is to be held uniform to 10 percent, no more than 0.1 of the x-rays can be captured in the resist, and the highest sensitivity achievable with a 0.5 μm resist thickness (maintaining 0.1 μm resolutions) is ∿ 5 mj/cm^2.

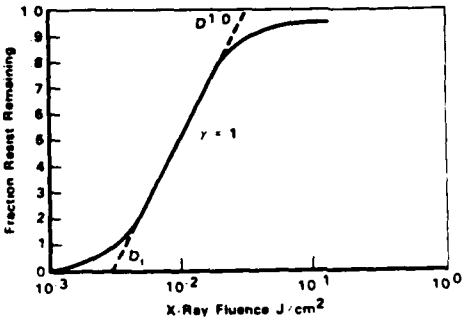

Figure 10. Hypothetical thickness after exposure for negative resist

Table 2. System Parameters

Laser	Quantel 402 DP .3 J/pulse, 10 Hz, τ = .2 nsec, λ = 1.06 μm, D_b = .95 cm, Δ = 7 x 10^{-4} rad
Lens	3 cm focal length
Target	Copper cylinder
Window	Differentially pumped orifices
Mask substrate	2.5 μm SiC
Mask Absorber	.2 μm Au
Target/mask distance	5 cm
Mask/wafer distances	40 μm
Exposure system	Step and repeat
Step exposure area	4 cm^2, 2 cm x 2 cm
Resist	Sensitized, doped copolymer

Assuming a resist with a sensitivity of 5 mj/cm^2 and the system of Table 2, the exposure time for each step is 6.5 seconds, giving a throughput of 1.6 cm^2/sec, neglecting repositioning time.

Conclusions

The laser-plasma x-ray source has a very high average brightness, only about a factor of ten lower than the Spear synchroton at 1 keV. However, the high brightness achieves its maximum advantage only when the resolution is limited by the source penumbra. Thus, the laser-plasma source compares best with conventional sources for high resolution applications. It should be expected that as IC demands require resolution of 0.1 μm or better that this type of source will be increasingly beneficial.

Additional improvements in the average power of commercial high brightness lasers as well as new developments in soft x-ray resists should also make the laser-plasma x-rays source useful for lithography in the μm range.

References

(1) H. I. Smith, D. L. Spears, and S. E. Bernacki, J. Vac. Sci. Technol., 10, 913 (November-December, 1973).

(2) N. D. Wittels, Fine Line Lithography, Chapter 1, R. Newman, ed., North-Holland (1980).

(3) A. Zacharias, Solid State Tech., 57-59 (August, 1981).

(4) J. R. Maldonado, M. E. Poulsen, T. E. Saunders, F. Vratny, and A. Zacharias, J. Vac. Sci. Technol., 16, 1942 (November-December, 1979).

(5) H. M. Epstein, P. J. Mallozzi, and B. E. Campbell, SPIE, 385, 141 (1983).

(6) P. J. Malozzi, H. M. Epstein, and R. E. Schwerzel, In Adv. in X-Ray Analysis, G. J. McCarthy et al, Eds., 22, 267 (1979).

(7) D. J. Nagel, Annals N.Y. Acad. Sci., 342, 235 (June, 1980).

(8) D. J. Nagel, M. C. Peckerar, R. R. Whitlock, J. R. Greig, and R. E. Pechacek, Electronics Lett., 14, 781 (1978).

(9) H. M. Epstein, R. L. Schwerzel, and B. E. Campbell, 6th International Workshop on Laser Interactions and Related Plasma Phenomena, eds., G. H. Miley and H. H. Hora, Plenum (1983).

(10) R. McCorkle, J. Angilello, G. Coleman, R. Feder, and S. J. La Placa, Science, 205, 401 (1979).

(11) P. L. Mallozzi, H. M. Epstein, R. G. Jung, D. C. Applebaum, B. P. Fairand, and W. J. Gallagher, Fundamental and Applied Laser Physics: Proceedings of the Esfahan Symposium, M. S. Feld, A. Javan, and N. A. Warnick, eds., John Wiler & Sons, Inc. (1973).

(12) E. Spiller and R. Feder, X-Ray Lithography, Chapter 3, H. J. Queisser, e., Springer-Verlag (1977).

(13) R.W.P. McWhirter, Plasma Diagnostic Techniques, Chapter 5, R. H. Huddlestone and S. L. Leonard, eds., Academic Press, New York, New York (1965).

(14) J. M. Eggleston, L. J. Kane, J. Outeruchrer, and R. L. Byer, Opt. Lett. 7, 405 (1982).

(15) J. D. Myers, Kigre, Inc., private communications.

(16) R. K. Watts, Solid State Techn., 68-71 and 82 (May, 1979).

(17) V. A. Boiko, A. Ya Vainer, K. M. Dyumaev, S. A. Kireeva, V. F. Limanova, I. Ya Skobelev, A. Ya Faenov, and S. Ya Khakhalin, Sov. Phys. Tech. Phys., 27 (11) (November, 1982).

(18) G. N. Taylor and T. M. Wolf, J. Electrochem. Sci., 127, 2665 (December, 1980).

END

DTIC

9-86